Visual system development of the spotted unicornfish, *Naso brevirostris* (Acanthuridae)

Valerio Tettamanti[1,2], Fanny de Busserolles[1], David Lecchini[3,4], N. Justin Marshall[1], Fabio Cortesi[1]

[1] Queensland Brain Institute, The University of Queensland, 4072 Brisbane, Australia

[2] Swiss Federal Institute of Technology Zurich, 8092 Zurich, Switzerland

[3] PSL Research University: EPHE-UPVD-CNRS, USR3278 CRIOBE, BP 1013, 98729 Papetoai, Moorea, French Polynesia

[4] Laboratoire d'Excellence "CORAIL", Paris, France

Corresponding author: F. Cortesi, E-mail: fabio.cortesi@uqconnect.edu.au

Summary statement

Tettamanti et al. uncover changes in retinal topography as well as opsin gene expression during the ontogeny of the spotted unicornfish, *Naso brevirostris*.

Keywords: visual ecology, teleosts, fish, ontogeny, opsin, retina, visual acuity

Abstract

Ontogenetic changes of the visual system are often correlated to shifts in habitat and feeding behaviour of animals. Coral reef fishes begin their lives in the pelagic zone and then migrate to the reef. This habitat transition frequently involves a change in diet and light environment as well as major morphological modifications. The spotted unicornfish, *Naso brevirostris*, is known to shift diet from zooplankton to algae and back to mainly zooplankton when transitioning from larval to juvenile and then to adult stages. Concurrently, *N. brevirostris* also moves from an open pelagic to a coral-associated habitat before migrating up in the water column when reaching adulthood. Using retinal mapping techniques, we discovered that the distribution and density of ganglion and photoreceptor cells in *N. brevirostris* mostly changes during the transition from the larval to the juvenile stage, with only minor modifications thereafter. Similarly, visual gene (opsin) expression based on RNA sequencing, although qualitatively similar between stages (all fishes mainly expressed the same three cone opsins; *SWS2B, RH2B, RH2A*), also showed the biggest quantitative difference when transitioning from larvae to juveniles. The juvenile stage in particular seems mismatched with its reef-associated ecology, which may be due to this stage only lasting a fraction of the lifespan of these fishes. Hence, the visual ontogeny found in *N. brevirostris* is very different from the progressive changes found in other reef fishes calling for a thorough analysis of visual system development of the reef fish community.

Introduction

Many animals use vision to perform important behavioural tasks such as feeding, mating, avoiding predators and to find a suitable home (Cronin et al., 2014). At the core of the vertebrate visual system is the retina, an extrusion of the brain which is subdivided into various functional layers, two of which are at the centre of this study, the photoreceptor layer and the ganglion cell layer.

The photoreceptor layer is the first stage of visual processing and is composed of morphologically diverse cone and rod photoreceptor cells which absorb light, transform it into an electrical signal, and send the information downstream to various neural cells via the phototransduction cascade. Cones mediate vision in bright light conditions and colour vision while rods mediate vision in dim light conditions (Walls, 1942). Cones can further be classified into different types depending on their morphology and/or the type of photopigment (an opsin protein covalently bound to a light absorbing chromophore) they possess (Hunt et al., 2014). Morphologically, cones can be classified as single, double, triple or quadruple, although only the first two configurations are common and are often arranged in regular and specific patterns or mosaics (Bowmaker and Kunz, 1987; Peichl et al., 2004). Molecularly, cones are also classified into four types based on the opsin genes they express that encode for different protein classes sensitive to different parts of the visible light spectrum: The short-wavelength protein class 1 opsin (SWS1) maximally sensitive to UV-violet wavelengths (355-450 nm λ_{max}), a second short-wavelength class opsin (SWS2) maximally sensitive to the violet-blue part of the spectrum (410-490 nm λ_{max}), a middle-wavelength class 2 opsin (RH2) maximally sensitive to blue-green wavelengths (435-535 nm λ_{max}), and a long-wavelength class opsin (LWS) maximally sensitive to the green-red part of the light spectrum (490-625 nm λ_{max}) (Bowmaker, 2008; de Busserolles et al., 2017; Torres-Dowdall et al., 2017). In percomorph fishes, SWS proteins are found in single cones, whereas RH2 and LWS opsins occur in double cones (Hunt et al., 2014). Most vertebrates possess a single type of rod photoreceptor expressing the rod opsin protein (RH1; 460-530 nm λ_{max}; Bowmaker, 2008), but see Musilova et al., 2019 for deep-sea fishes with multiple RH1's that extend their sensitivities to ~ 440 nm λ_{max}.

The ganglion cell layer is the last stage of visual processing in the retina and is composed of ganglion cells that possess axons that reach to the inner surface of the retina and converge into the optic nerve to send the information into the central nervous system (Walls, 1942). Therefore, the arrangement and the spacing between one ganglion cell to another is one of the determining factors of visual acuity (or resolution) (Fernald, 1988).

In order to perform at its optimum, the visual system of a particular species is adapted to the type of habitat they live in and to the prevailing surrounding light conditions (Lythgoe, 1979). In general, vertebrates range from cone-monochromats with a single spectral class of cone photoreceptor (e.g., sharks and many rays), over di- and trichromats (e.g., most mammals and many marine fishes), to tetrachromats (e.g., most birds and many freshwater fishes; Bowmaker 2008). Cone photoreceptors and their respective opsin repertoires are particularly diverse in teleost fishes (e.g., Lin et al., 2017; Musilova et al., 2019). This is thought to primarily be due to the different light environments fishes inhabit (Cronin et al., 2014; Lythgoe, 1979), but in some instances may also be driven by sexual selection (Endler, 1990) and/or the feeding habits of species. For example, UV photoreception increases feeding efficiency in some fishes eating UV-absorbing or scattering zooplankton (Flamarique, 2016; Loew et al., 1993; Browman et al., 1994), while herbivorous fishes may profit from visual systems tuned to longer wavelengths due to the red-reflecting properties of chlorophyll (Cortesi et al., 2018 preprint; Marshall et al., 2003; Stieb et al., 2017).

Moreover, the density of photoreceptors and ganglion cells can also vary not only between species, but also within an individual's retina over its lifespan (Shand et al., 1999, 2000). The study of their distribution using the wholemount technique (Coimbra et al., 2006; Stone and Johnston, 1981; Ullmann et al., 2012) provides useful information on the visual ecology of a species, which usually reflects its habitat and behavioural ecology (Bozzano and Collin, 2000; Collin and Pettigrew, 1988a,b; Collin and Pettigrew, 1989; Hughes et al., 1977). Two main specializations can be found in vertebrates: area and streaks, (Collin and Pettigrew, 1988a,b). Both specializations have higher densities of cells compared to the rest of the retina, resulting in regions of acute vision in the corresponding field of view. An area is a concentric increase in cell density in a particular region of the retina, in some vertebrates it is termed a fovea due to other structural adaptations (Walls, 1942). In teleost fishes, areas are often located temporally (i.e., area temporalis) and found in species that live in enclosed environments such as caves or coral structures, and/or coral overhangs (Collin and Pettigrew, 1989; Collin and Shand, 2003). The temporal area receives the visual information from the frontal field of view, corresponding to the natural swimming direction of fishes. Nevertheless, multiple area centralis can also be found in a single retina (Collin and Pettigrew, 1989). For example, Triggerfishes (Balistidae) possess an area in both the nasal and temporal part of the retina, which correlates with two main visual tasks: feeding (temporal) and predator avoidance (nasal) (Collin and Pettigrew, 1988b; Ito and Murakami, 1984).

A horizontal streak is defined by an increase in cell density along the meridian. Most horizontal streaks are found in the central meridian, but sometimes they can also be located more ventrally or dorsally (Collin and Shand, 2003). The streak maintains a high spatial resolving power throughout the horizontal section of the retina and is thought to be used to scan the horizon. It leads to an elongated sampling of the visual environment without continuous eye movements (Collin and Shand, 2003). Teleost fishes possessing a horizontal streak are commonly found in open water environments such as sandy bottoms or pelagic open ocean environments (Collin and Pettigrew, 1988b).

Variability in retinal structure and opsin gene repertoire does not only exist between species but both visual features may also change throughout the life of an individual. This is especially true for species that undergo substantial habitat changes during ontogeny such as coral reef fishes. The life of most coral reef fishes starts in the shallower zone of the open ocean as larvae (Helfman et al., 2009; Job and Bellwood, 2000), where resources may be high and the risk of predation is low (Fortier and Harris, 1989). At this stage, pelagic fish larvae feed typically on zooplankton (Boehlert, 1996) and rely on vision primarily for fundamental tasks such as predator avoidance and feeding (Leis and Carson-Ewart, 1999). After their oceanic phase, reef fish larvae typically find a suitable coral reef patch to settle on and again vision is one of the main senses used (Lecchini et al., 2005a,b). During this settlement phase, reef fish larvae undergo metamorphosis and reach the juvenile stage in which they usually already possess all basic morphological features of the adult form (Holzer et al., 2017). Following settlement on the reef, juvenile fishes are challenged with visual cues that are much more complex than in the open ocean varying both in chromaticity and luminance. Hence, at this stage (or slightly before – Cortesi et al., 2016) the visual system of coral reef fishes is expected to undergo changes both in morphology and physiology (Helfman et al., 2009).

To date, changes in arrangement (i.e., mosaic) and distribution of the photoreceptor cells throughout ontogeny have been documented only in few coral reef fishes (Shand, 1997). These changes are thought to enhance survivability by increasing feeding success and facilitate predator avoidance in reef stages (juveniles and adults; Shand, 1997). Along with changes in morphology, ontogenetic changes in opsin gene expression have also been reported from a handful of species (Cortesi et al., 2015b, 2016). For example, in the dottyback *Pseudochromis fuscus*, the number and type of opsin genes that are expressed differs between larval, juvenile, and adult stages. Along with the change in opsin gene expression, the visual system may also transform to more complex colour processing

capability, such as di- to tri-chromacy or even up to tetrachromacy. This increase in chromaticity ultimately requires behavioural testing to confirm and is likely to reflect major habitat transitions throughout development equipping e.g., dottybacks with a more complex visual system as they grow and mature (Cortesi et al., 2015b, 2016). In comparison, while some freshwater cichlid species show a similarly dynamic change in opsin gene expression through ontogeny, other species do not change gene expression much (neoteny) or then, they directly develop from the larval to the adult gene-expression pattern (Carleton et al., 2008; Härer et al., 2017). We currently do not know whether a progressive developmental change of the visual system, as e.g., found in the dottyback (Cortesi et al., 2016), is a common feature shared among reef fishes, or whether some species also show different developmental modes, similar to what is found in cichlid fishes.

In this study we investigated ontogenetic changes in retinal topography and opsin gene expression in three life stages (larval, juvenile, adult) of the spotted unicornfish, *Naso brevirostris* Cuvier 1829, from the surgeonfish family (Acanthuridae) (Fig. 1). *N. brevirostris* is known to shift both diet and habitat during ontogeny (Choat et al., 2002; Randall et al., 1997). Pelagic larvae feed on zooplankton before settling on the reef where they mainly feed on algae as juveniles. As adults, *N. brevirostris* migrate to the reef slope returning to a mostly zooplanktivorous diet (Choat et al., 2002, 2004; Randall et al., 1997). We therefore hypothesized that the visual system of *N. brevirostris* would show a 'classic' developmental mode, linked to either changes in habitat or diet, or both, and with a progression from larval, to juvenile and finally adult traits. Moreover, *N. brevirostris* develops an elongated rostral snout during maturation, and this prominent morphological change may also affect its visual requirements as it might obstruct the visual field of the fish.

Materials and methods

Study species and collection

Individuals of *N. brevirostris* were collected on the Northern Great Barrier Reef, Australia, under the Great Barrier Reef Marine Park Association (GBRMPA) permits G17/38160.1 and G16/38497.1, Queensland Fisheries permit #180731, or in French Polynesia. Adults [n = 5; standard length (SL): range = 27.7 – 33 cm, mean ± standard deviation = 30.4 ± 1.9 cm] were collected with a spear gun from No Name Reef (14°65 ′S, 145°65′E) on the outer Great Barrier Reef, Australia, in February 2018. Juveniles (n = 8; SL, 6.5 – 19.5 cm, 14.5 ± 3.7 cm) were collected using barrier nets, spear guns or clove oil and hand nets from reefs surrounding Lizard Island (14°40′S, 145°27′E) on the Great Barrier Reef between February

2016 – February 2018, and one juvenile fish was acquired through the aquarium supplier Cairns Marine (http://www.cairnsmarine.com/). Larval fish (n = 5; SL: 3.1 – 3.3 cm, 3.1 ± 0.1 cm) were captured using a crest net on Tetiaroa Island, French Polynesia (16°99′S, 149°58′W) in March 2018 (Besson et al., 2017; Lecchini et al., 2004). All animals were quickly anaesthetised following the NHMRC Australian Code of Practice under an animal ethics protocol of The Queensland Brain Institute (QBI/236/13/ARC/US AIRFORCE and QBI/304/16).

Each individual was photographed with a ruler in the frame, to be able to extract the standard length later on using Fiji v.1.0 (Schindelin et al., 2012). The eyes were enucleated and the cornea and lens removed using micro-dissection scissors. A small dorsal cut was made to keep track of the eye's orientation. The samples collected for retinal mapping were fixed in 4% paraformaldehyde in 0.1 M phosphate buffer (PBS; pH 7.4) and stored at 4 degrees Celsius and the eyes used for RNA sequencing were kept in RNAlater (Sigma) and stored at -20 degrees Celsius. For each eye, the lens diameter was measured after dissection and fixation.

Preparation of retinal wholemounts

Retinal wholemounts were prepared according to standard protocols (Coimbra et al., 2006, 2012; Stone and Johnston, 1981). Briefly, each eye cup was cut radially multiple times, to flatten it on a microscopy glass slide without damaging the tissue. The retina was oriented using the falciform process that extends ventrally. The sclera and choroid were gently removed and the retinas where bleached overnight in the dark at ambient temperature in a 3% hydrogen peroxide solution (in PBS). Large-sized adult retinas, that have a more developed retinal pigment epithelium, were bleached in the same solution but with a few drops of potassium hydroxide (Ullmann et al., 2012). While potassium hydroxide accelerates the bleaching process by increasing the pH of the solution, this type of bleaching is quite aggressive for the tissue. Therefore, these retinas were only bleached for 2-3h in the dark.

For ganglion cell analyses, retinas were mounted ganglion cell layer facing up on a gelatinized slide and left to dry overnight at room temperature in formalin vapours (Coimbra et al., 2006, 2012). Wholemounts were then stained in 0.1% cresyl violet (Nissl staining) following the protocol of Coimbra et al. (2006) and then mounted with Entellan New (Merck). Shrinkage of the retina using this technique is usually deemed negligible and, if present, restricted to the borders of the retina (Coimbra et al., 2006). In this study however, all the retinas were not equal in shrinkage due to major differences in retina size between

developmental stages. As such, the smaller retinas (larval stage) were more affected by shrinkage, due to their smaller surface (i.e., higher proportion of retinal borders), than the other stages (adult and juvenile stages). Shrinkage in these retinas was easily identified under the microscope and was taken into consideration in the data interpretation.

For photoreceptor analyses, retinas were wholemounted in 80% glycerol in 0.1M phosphate buffer, on non-gelatinized slides with the inner (vitreal) surface facing downwards. Contrary to ganglion cell mounting, photoreceptor mounting shows negligible shrinkage as it takes place in an aqueous medium (Peichl et al. 2004).

Stereological analyses and construction of topographic maps

The topographic distribution and the total number of ganglion cells, single cones, double cones and total cones in the three life stages of *N. brevirostris* were assessed using the optical fractionator technique (West et al., 1991), modified for wholemount retina use, by Coimbra et al., 2009, 2012. A computer running the Stereo Investigator software (v2017.01.1 (64-bit), Microbrightfield, USA) coupled to a compound microscope (Zeiss Imager.Z2) equipped with a motorized stage (MAC 6000 System, Microbrightfield, USA) and a digital colour camera (Microbrightfield) was used for the analysis. The contour of each retina wholemount was digitalized using a x5 objective (numerical aperture 0.16) and cells were counted randomly and systematically using a x63 oil immersion objective (numerical aperture 1.40) and the parameters summarised in Table S1. The total number of cells for each sample was then estimated by multiplying the sum of the neurons (ganglion cells or photoreceptors) counted by the area of sampling fraction (Coimbra et al., 2009; West et al., 1991).

The counting frame and grid size were chosen carefully in order to achieve an acceptable Shaeffer's coefficient of error (CE), while maintaining the highest level of sampling. The CE measures the accuracy of the estimation of the total cell number and it is deemed acceptable below 0.1 (Glaser and Wilson, 1998; Slomianka and West, 2005). The counting frame was adjusted between life stages to reach an average count of around 40 and 80 cells per sampling site for ganglion cells and photoreceptors respectively, but was kept identical for individuals of the same life stage (Table S1). Since fish of similar life stages can have a wide variation of standard lengths, the grid size was adjusted for all individuals to allow sampling of around 200 sites (± 10%) (de Busserolles et al., 2014a,b).

Three cell types can be found in the ganglion cell layer: ganglion cells, displaced amacrine cells and glial cells. These can usually be distinguished based on cytological criteria (Collin, 1988; Collin and Pettigrew, 1988c; Hughes, 1975) with ganglion cells having an

irregular shape, an extensive nucleus, and a larger size compared to smaller, rounder amacrine cells, which have a darker stained appearance, and glial cells having an elongated shape relative to the other two cell types (Fig. 2A). However, since amacrine cells were often difficult to distinguish from ganglion cells in *N. brevirostris*, especially in high density areas, amacrine cells were included in all counts and only glial cells were excluded. The inclusion of amacrine cells in the analysis should not interfere with the overall topography, since the distribution of amacrine cells has been shown to match the ganglion cell distributions in other animals (Bailes et al., 2006; Coimbra et al., 2006; Collin, 2008; Collin and Pettigrew, 1988c; Wong and Hughes, 1987), and the density of displaced amacrine cells in *N. brevirostris* was relatively low. However, the inclusion of amacrine cells in the ganglion cell counts will contribute to a slight overestimation of ganglion cell densities and ultimately to a slight overestimation of spatial resolving power. For ganglion cell analysis, a sub-sampling was performed in the regions of highest cell density to allow a more accurate estimation of the peak ganglion cell density. The same counting frame parameters as for the whole retina were used for the sub-sampling, but the grid size was reduced by half.

Photoreceptor cells, on the other hand, could be distinguished unambiguously into single and double cones (Fig. 2B). Both cone types were counted separately and simultaneously using two different markers to acquire data for single cones alone, double cones alone and total cones (single and double cones).

Topographic maps were created using the statistical program R v.3.4.1 (R Foundation for Statistical Computing, 2012) with the results exported from Stereo Investigator and the R script provided by Garza-Gisholt et al., 2014. As for previous retinal topography studies on teleost fishes (Dalton et al., 2016; de Busserolles et al., 2014a,b), the Gaussian Kernel Smoother from the Spatstat package (Baddeley and Turner, 2005) was chosen and the sigma value was adjusted to the distance between points (i.e., grid size) for each map (Fig. 3).

Spatial resolving power estimation

The upper limit of the spatial resolving power (SRP) in cycles per degree was estimated for each individual using the ganglion cell peak density as described by Collin and Pettigrew, 1989. The following formula was used:

$$\alpha = arctan\,(1/f)$$

where α is the angle subtending 1 mm on the retina and calculated assuming that f, the focal length of the fish, is 2.55 times the lens radius, the standard for teleost fishes according to the

Matthiessen ratio (Matthiessen, 1882). Then, knowing α, the peak density of ganglion cells (PDG in cells/mm) and the fact that two ganglion cells are needed to distinguish a visual element from its neighbouring element, the SRP in cycles per degree can be calculated as follow:

$$SRP = (PDG/\alpha)/2$$

Transcriptome sequencing, quality filtering, and de-novo assembly

The retinas from different life stages of *N. brevirostris* (adult, n = 3; juvenile, n = 6; larvae, n = 3) were dissected out of the eye cup, total RNA was extracted, and their retinal transcriptomes were sequenced according to Musilova et al. (2019). Briefly, total RNA of larval and smaller juvenile retinas was extracted using the RNeasy Mini Kit (Qiagen), and for larger juvenile and adult retinas the RNeasy Midi Kit (Qiagen) according to the manufacturer's instructions, which included a DNAse treatment. Total RNA concentration and quality were determined using an Eukaryotic Total RNA NanoChip on an Agilent 2100 BioAnalyzer (Agilent Technologies). Juvenile transcriptomes were sequenced in-house at the Queensland Brain Institute's sequencing facility. For these samples, strand-specific libraries were barcoded and pooled at equimolar ratios and sequenced at PE125 on a HiSeq 2000 using Illumina's SBS chemistry version 4. Library preparation (strand-specific, 300 bp insert) and transcriptome sequencing (RNAseq HiSeq PE150) for larval and adult individuals was outsourced to Novogene (https://en.novogene.com/).

Retinal transcriptomes were filtered, and *de novo* assembled following the protocol described in de Busserolles et al. (2017). Briefly, raw-reads of transcriptomes were uploaded to the Genomics Virtual Laboratory (GVL 4.0.0) (Afgan et al., 2015) on the Galaxy Australia server (https://usegalaxy.org.au/), filtered by quality using Trimmomatic (Galaxy Version 0.36.4) (Bolger et al., 2014) and then *de novo* assembled using Trinity (Galaxy Version 2.4.0.0) (Haas et al., 2013).

Opsin gene mining and phylogenetic reconstruction

Following the protocol in de Busserolles et al. (2017), the *N. brevirostris* transcriptomes were mined for their visual opsin genes. Briefly, using the opsin coding sequences from the dusky dottyback, *Pseudochromis fuscus* (Cortesi et al., 2016), we searched for the *N. brevirostris* opsin genes by mapping the de-novo assembled transcripts to the *P. fuscus* reference genes using Geneious v.11.1.3 (www.geneious.com). *P. fuscus* was chosen because it is relatively

closely related to *N. brevirostris*, and because it possesses orthologs from all of the ancestral vertebrate opsin genes (Cortesi et al., 2016).

Assemblies based on short-read libraries tend to overlook lowly expressed and similar gene copies and/or short-reads may be misassembled (chimeric sequences); for that reason, a second approach was used to confirm the visual opsin genes of *N. brevirostris.* A manual extraction of the gene copies was performed by mapping raw-reads against the *P. fuscus* references and then moving from single nucleotide polymorphism (SNP) to SNP along the gene taking advantage of paired-end information to bridge gaps between SNPs. The extracted reads were then de-novo assembled and their consensus was used as template against which unassembled reads were re-mapped to elongate the region of interest; this approach eventually lead to a reconstruction of the whole coding region (for details on this approach, see de Busserolles et al., 2017; Musilova et al., 2019).

Opsin gene identity was then confirmed using BLAST (http://blast.ncbi.nlm.nih.gov/) and by phylogenetic reconstruction to a reference dataset obtained from Genbank (www.ncbi.nlm.nih.gov/genbank/) and Ensembl (www.ensembl.org/) (as per de Busserolles et al., 2017; Fig. 4, Fig. S4). The opsin gene phylogeny was obtained by first aligning all opsin genes i.e., the reference dataset and *N. brevirostris* genes using the L-INS-I settings as part of the Geneious MAFFT plugin v.1.3.7 (Katoh and Standley, 2013). jModeltest v.2.1.10 (Darriba et al., 2012) was subsequently used to select the most appropriate model of sequence evolution based on the Akaike information criterion. MrBayes v.3.2.6 (Ronquist et al., 2012) as part of the CIPRES platform (Miller et al., 2010) was then used to infer the phylogenetic relationship between opsin genes using the following parameter settings: GTR+I+G model; two independent MCMC searches with four chains each; 10 million generations per run; 1000 generations sample frequency; and, 25% burn-in.

Opsin gene mining and phylogenetic reconstruction revealed, amongst a number of other visual opsin genes, two *N. brevirostris RH2* paralogs of which one clustered within the *RH2A* clade of other percomorph fishes. However, the phylogenetic placement of the second paralog could not fully be resolved using this approach alone (Fig. 4). Therefore, in order to resolve a more detailed relationship between the two *N. brevirostris RH2* paralogs, we took advantage of the phylogenetic signal within the single exons of the displaced paralog (as per Cortesi et al., 2015b). The five *N. brevirostris RH2-2(B)* exons were obtained by annotating the coding regions of the gene with a *P. fuscus RH2* ortholog. The single exons were separated from one another and inserted as "single genes" in the alignment in a reduced (*RH2* genes only) reference dataset, along with the *N. brevirostris RH2A* gene. The *RH2* specific

phylogeny was then reconstructed using MrBayes on the CIPRES platform using the same parameters as before (Fig. 5A).

To support our phylogenetic analyses, the amino acid sequences of the RH2 paralogs were aligned to the amino acid sequence of bovine rhodopsin (Genbank accession NM001014890) using MAFFT in Geneious with parameters: L-INS-I, BLOSUM62, gap open penalty 1.53, offset value 0.123. Referring to bovine rhodopsin as the reference, this allowed us to compare site 122 between RH2s, which has been found key to distinguish between longer- (RH2A in percomorphs) and shorter-shifted (RH2B in percomorphs) RH2 copies (Chinen et al., 2005; Fig. 5C).

Opsin gene expression

Quantitative opsin gene expression was assessed by mapping the filtered reads to the assembled coding regions of the *N. brevirostris* opsin genes as per de Busserolles et al. (2017). This methodology was used for each individual of the three life stages. Proportional opsin expression for single cones (p_i ; SC) and double cones (p_i ; DC) for each gene (i) was then calculated by first normalizing the number of reads of each gene (R_i) to the length of each gene specific coding region/sequence (cds):

$$NR_i = (R_i/bp_i)$$

where, R is the number of reads and bp_i the number of base pairs in the cds of a gene i which was used to normalize the data between the opsins. The proportion of opsin expressed, out of the total normalized expression for single (Tot_{SC}) and double cones (Tot_{DC}), was then calculated separately. The following formulas were used, depending on the type of cone gene i was expressed in:

$$p_i\ ;\ SC = NR_i\ /\ (Tot_{SC}) \qquad \text{or} \qquad p_i\ ;\ DC = NR_i\ /\ (Tot_{DC})$$

We also calculated the proportional expression of the rod opsin compared to total normalized opsin expression (Tot_{Opsin}):

$$p_i\ ;\ Rod = NR_i\ /\ (Tot_{Opsin})$$

Results

Topographic distribution of ganglion cells and spatial resolving power

Topographic maps of ganglion cells (including amacrine cells) for the three life stages of *N. brevirostris* were constructed from Nissl-stained retinal wholemounts. Little variation in topographic distribution of ganglion cells was observed within the same ontogenetic stage. Therefore, only the topographic map of one individual per life stage is presented here (Fig. 3A), and the results for the remaining individuals are shown in Supplementary Fig. S1.

Differences in retinal topography were mainly found between the larval stage and the two later stages (Fig. 3A). In general, the larval retina showed less specializations compared to juvenile and adult retinas. In the larval retina, an onset of a horizontal streak was observed with the highest cell density found in the central meridian of the retina (1.5x increase compared to the areas with the lowest cell densities). Within this weak streak, three areas of high cell densities were found; in the nasal, central and temporal parts of the retina. However, these areas of high cell densities are to be taken with caution due to the limitations of the Nissl-staining protocol for very small retinas. Larval retinas were challenging to prepare and analyse due to their small size and thus, the higher amount of shrinkage present after staining. After several attempts with different larvae, only one larval retina was deemed acceptable for analysis. Even for this individual, the areas of high cell densities in the nasal and temporal part of the retina are questionable, since they are very close to the retinal borders and therefore could be the result of shrinkage. A prominent horizontal streak along with a centralized area centralis (the area centralis had a 2.5-3x increase in cell density compared to the areas with the lowest cell densities) was present in the juvenile and adult individuals. Similarly to the larvae, the streak in juveniles and adults was located on the central meridian of the retina extending to the nasal and temporal margins. Although slightly different patterns were found for each life stage, they all showed a higher ganglion cell density in the central area close to the optic nerve, accompanied by a horizontal streak (Fig. 3A).

The total number of ganglion cells increased with the size of fish and ranged from 208,975 cells for the larval individual, over ~1,600,000 cells for juveniles, to ~2,100,000 cells for adults (Table 1). Conversely, the mean cell density decreased with the size of the fish ranging from 19,439 cells/mm^2 in the larval individual, over ~8,500 cells/mm^2 in juveniles, to ~5,000 in cells/mm^2 in adults. Peak cell density also decreased through development, from 30,400 cells/mm^2 in the larval individual, to ~23,000 cells/mm^2 in juveniles, and ~ 20,500 cells/mm^2 in adults.

Based on the peak of ganglion cells densities, the SRP of *N. brevirostris* ranged from 2.98 cycles per degree in the larval individual, over ~8.0 cycles per degree in juveniles, to a maximum of 11.0 cycles per degree in adults (Table 1). Overall, SRP or visual acuity in *N. brevirostris* increased with the size of the fish with very little variation found within ontogenetic stages (Fig. S2).

Topographic distribution of cone photoreceptors

The density and topographic distribution of cone photoreceptors (double and single cones), was assessed in the three life stages of *N. brevirostris*. Double and single cones were arranged in a square mosaic, with one single cone at the centre of four double cones (Fig. 2B). This pattern was consistent throughout the entire retina, thus providing a ratio of double cones to single cones of 2:1. As a consequence of this regular arrangement, the topographic distribution of single cones, double cones and total cones was identical. Moreover, similar to the ganglion cell topography, little variation in topographic distribution of cone photoreceptors was observed within the same ontogenetic stage. Therefore, only the total cone topographic map of one individual per life stage is presented here (Fig. 3B). The remaining maps (i.e., for single and double cones separately, and maps of all individuals) are provided in the Supplementary Fig S3 and on Dryad.

The topographic distribution of cone photoreceptors varied between stages with a continuous increase in specialization from the larval to the adult stage (Fig. 3B). Larvae had a weak horizontal streak in the central meridian with two large areas of high cell density in the nasal part and the temporal part of the retina. One of the two analysed larval individuals also showed a dorsal increase in cell density (Fig. S3f). However, this apparent increase in cell density was likely caused by an artefact from not properly flattening the dorsal part of the retina during mounting and should therefore be disregarded. Compared to the larvae, juveniles had a more pronounced horizontal streak in the central meridian with a peak density of cells in the temporal part of the retina. Moreover, a weak vertical streak could be seen in the temporal part of the retina, extending from the dorso-temporal area to the ventral-temporal area. In adults, the horizontal streak in the central meridian was still present but did not extend as far into the nasal part as in the juveniles. Moreover, the vertical streak was more prominent compared to the one found in juveniles resulting in a very large area of high cell density in the temporal region (Fig. 3B). The continuous nature of the transition between juvenile and adult specializations is highlighted by the topography of individuals of intermediate sizes (Fig. S3). For example, the horizontal streak was less pronounced in the

nasal part of a larger (SL 19.5 cm; Fig. S3c) compared to a smaller juvenile (SL 13.8 cm; Fig. S3d). Conversely, the vertical streak in a smaller adult (SL 27.7 cm; Fig. S3b) was still developing compared to the one found in a larger adult (SL 29.7 cm; Fig. S3a).

Similar to the ganglion cells (Table 1), the total number of photoreceptors increased with the size of the fish ranging from ~650,000 cells in larvae, over ~4,300,000 cells in juveniles, to ~5,700,000 cells in adults (Table 2). A large difference in the total number of photoreceptors was found between the two juvenile individuals. This difference is likely due to the size difference between these individuals. Photoreceptor peak cell densities decreased with the size of the fish, ranging from ~69,000 cells/mm^2 in larvae, over ~51,000 cells/mm^2 in juveniles, to ~34,000 in cells/mm^2 in adults (Table 2).

The total number of cone photoreceptors was greater compared to the total number of ganglion cells, indicating a high summation ratio between the two cell types. For one individual (juvenile ID3), the distribution of both ganglion cells and photoreceptors were analysed, which allowed us to estimate the summation ratio between photoreceptors and ganglion cells in low- and high-density areas, respectively. For this individual, the summation ratio was found to be as low as 2.3 in the central part and as high as 5.4 in the ventral-temporal part of the retina.

Visual opsin genes and their expression in Naso brevirostris

N. brevirostris were found to mainly express four opsin genes in their retinas. Independent of ontogeny, these were the 'blue-violet' *SWS2B*, the 'greens' *RH2B* & *RH2A*, and the rod opsin *RH1*. The 'red' *LWS* was also found to be expressed, albeit at very low levels in all stages (0.1 – 6.5 % of total double cone opsin expression; Fig. 6A, Table S2). The phylogenetic reconstruction based on the full coding regions of the genes confirmed the positioning of all genes within their respective opsin class (Fig. 4). However, for *RH2B* in particular the resolution between *RH2* specific clades was poor (Fig. 4, Fig. S4). This was resolved using the exon-based approach which showed the placement of some of the *N. brevirostris RH2B* exons within a greater percomorph *RH2B* clade (Fig. 5A). We also found evidence for substantial gene conversion affecting this gene with the placement of Exons 1 and 2 close to, or within, the *RH2A* clade (Fig. 5B). Amino acid comparison between the two RH2 paralogs corroborated our phylogenetic placement of genes and revealed the conserved sites E122 and Q122 for the longer- (RH2A) and shorter-shifted (RH2B) copies, respectively (Fig. 5C).

Quantitative opsin gene expression revealed that *SWS2B* was the only single cone gene and thus, expressed at 100% in all developmental stages (Table S2). Of the double cone

opsins, there was a change in expression for the *RH2* genes with ontogeny. During the larval stage (n = 3), *RH2B* (mean ± standard error, 36.2 ± 4.8%) was less highly expressed compared to *RH2A* (63.6 ± 4.8%). The opposite pattern was found in the juvenile (n = 6) and adult stages (n = 3), where *RH2B* was the highest expressed of all double cone opsins genes (juvenile: 56 ± 1.3%; adult: 56.1 ± 1.9%). *RH2A* in the juvenile (41.2 ± 1.4%) and adult (38.1 ± 1.6%) stages was less highly expressed. Despite *LWS* being lowly expressed in all stages, there was a noticeable increase in expression with development (larval: 0.2 ± 0.0%; juvenile: 2.8 ± 0.7%; adult 5.8 ± 0.4%; Fig. 6A). Rod opsin (*RH1*) expression was substantially higher compared to the cone opsin expression in all stages (82 – 86% for all stages; Fig. 6B).

Discussion

The visual systems of fishes often change through development when transitioning from one habitat to another. These changes are usually associated with a shift in light environment e.g., when moving from the open ocean to a coral reef, but possibly also with changes in diet and predation pressure (Sale, 2013). Our objective was to assess the visual system development in the spotted unicornfish, *N. brevirostris*. *N. brevirostris* experiences multiple changes in habitat, diet and morphology throughout ontogeny (from larval to adult stages; Fig. 1) making it a prime candidate to study visual system changes on the reef.

Ganglion cell topography

Retinal topography is an effective method to identify visual specializations and recognise the area of the visual field a species is most interested in (Collin, 2008; Collin and Pettigrew, 1988a; Hughes, 1977). In marine fishes, visual specializations have been found to correlate with the structure and symmetry of the environment they live in and/or with their feeding behaviour (Caves et al., 2017; Collin and Pettigrew, 1988a,b; Ito and Murakami, 1984; Shand, 1997). In this study we show that the *N. brevirostris* eye possesses a horizontal streak in all life stages (Fig. 3A). This type of specialization has previously been found in species living in open environments where an uninterrupted view of the horizon, defined by the sand-water or air-water interface, is present (Collin and Pettigrew, 1988b). Since *N. brevirostris* spends much of its life (larval and adult stages) searching for prey in the water column, having a pronounced horizontal streak is likely to increase feeding and predator surveillance capabilities by allowing it to scan the horizon without using excessive eye movements (Collin and Shand, 2003). Moreover, at the larval stage this type of specialization may also enable fish to scan the environment when searching for a reef habitat to settle on. On the contrary, a

horizontal streak does not seem to match the visual needs at the juvenile stage during which *N. brevirostris* lives in close association with the reef i.e., in a more enclosed 3D environment. At this life stage, we would have expected to find one (or multiple) area centralis and no horizontal streak; a common feature in fishes that live close to, or within the reef matrix (Collin and Pettigrew, 1988a,c). Compared to the lifespan of these fishes (up to 20 years), the juvenile stage is relatively short (~ 3 years; Choat and Axe, 1996), which may explain the maintenance of the horizontal streak throughout development.

The peak ganglion cell density in the juvenile and adult stages is found in the central part of the retina (i.e. at the centre of the streak, Fig. 3A). This is quite unusual, as the area of high cell density in coral reef fishes is normally found in the temporal zone where it receives information from the nasal visual field, and thus is usually correlated with feeding and predator avoidance in front of the fish (Collin and Pettigrew 1988a, 1989; Fritsch et al., 2003, 2017; Shand et al., 2000). The type of specialization found in *N. brevirostris* could potentially be associated with its unusual visual behaviour as fishes are found to examine objects side-on (V. Tettamanti, unpublished observations). A possible explanation for this peculiar behaviour is that due to its protruded snout, which grows through development, the frontal image might be partially blocked and stereoscopic vision may be impaired or even impossible (Purcell and Bellwood ,1993). Although the visual field of *N. brevirostris* was not investigated in their study, Brandl and Bellwood (2013) suggested that the protruded snout found in many *Naso* species indeed prevents an overlap of their horizontal field of view. Similar to the monocular vision found in hammerhead sharks (Lisney and Collin, 2008; McComb et al., 2009), increasing visual acuity in the central part of the retina would thus maximise a sideward oriented visual field. Together with a visual streak, a high cell density in the central part of the retina is likely to enable *N. brevirostris* to accurately navigate both within the complexity of the reef as well as in open water.

Photoreceptor topography

The photoreceptor topography showed a similar trend to the ganglion cell topography with bigger changes occurring between the larval and juvenile stage and only minor adjustments thereafter (Fig. 3B). In addition to a weak horizontal streak, larval fishes had two peaks of high cell densities in the nasal and temporal zones, which comply with two of their main ecological needs: feeding (temporal; looking forward) and predator avoidance (nasal; looking backwards) (Boehlert, 1996; Collin and Pettigrew, 1988a; Fortier and Harris, 1989). These high-density regions were not matched by the ganglion cell topography and as such, are

likely to provide areas of higher sensitivity (i.e., areas of high photoreceptor to ganglion cell ratio; Walls, 1942). Moreover, although larval fishes rely mainly on olfactory cues to zoom in on a suitable habitat for settlement (Lecchini et al., 2005b), the area of high cell densities in the temporal part in particular might also assist when searching for said habitat over longer distances (Mouritsen et al., 2013).

In addition to the horizontal streak becoming more prominent in juvenile and adult stage, *N. brevirostris* showed a temporal vertical specialization appearing at the juvenile stage and being more pronounced in adults (Fig. 3B). Such a double streak specialization, with a vertical and a horizontal component, is a first in coral reef fishes. *N. brevirostris* adults live on the coral reef slope/wall, and move up and down the wall (from 2 - 122 m) while foraging and searching for mates (Mundy, 2005). As such, in line with the terrain hypothesis (Hughes, 1977), the evolution of this vertical specialization is likely a result of the vertical component in their visual environment.

A difference in the topography of ganglion cells and photoceptors means that the summation ratio between the cell types i.e., the sensitivity and spatial resolution of the retina, also differs depending on the visual field in question. For example, high photoreceptor densities and comparable low ganglion cell densities in the ventral-temporal and dorsal-temporal parts of the vertical streak confer higher sensitivity to these two areas (Walls, 1942). Theoretically, this enables juvenile and adult *N. brevirostris* to detect even small differences in luminance, which may help to detect well camouflaged predators against the reef wall. A high density of both photoreceptor and ganglion cells found in the centre of the retina, on the other hand, confers a low summation ratio which leads to an increase in visual acuity (Walls, 1942). This area of high acuity may help fish to identify conspecifics and also to distinguish between food items (Cronin et al., 2014).

To summarize, retinal topography in *N. brevirostris* may be adapted to the habitat in both the larval and the adult stage. Juveniles live in a more enclosed, 3D coral reef environment compared to the other two life stages. Therefore, we would have expected the juvenile visual system to reflect its habitat by having a less developed streak and one or more area centralis instead. The unexpected topography found in the juvenile stage may be explained by this stage only lasting a fraction of the lifespan of *N. brevirostris* (Choat and Axe, 1996). The relatively short period of time spent in a habitat rich in shelter and food enables the fish to grow big enough to avoid most predators (Barnes and Hughes, 1999; Lasiak, 1986). During this time, juvenile *N. brevirostris* mostly feed on benthic algae, which do not require a highly specialized visual system in terms of retinal topography (Caves et al.,

2017; Collin and Pettigrew, 1988a,b; Randall et al., 1997). As such, instead of changing the visual system multiple times, it is likely more energy efficient to maintain (or slightly adjust) a visual system that is optimally adapted for both the larval and adult stages.

Visual acuity

The visual acuity of *N. brevirostris* was found to increase through development (Fig. S2; Table 1). This seems to be a common feature in coral reef fishes, as a higher acuity often correlates with an increase in eye size during growth. The benefit of having a higher visual acuity is that, as fishes grow and expand their home ranges, it increases the distance at which visual objects such as predators, conspecifics, and food can be detected (Caves et al., 2017; Shand, 1997). Accordingly, like in other coral reef fish larvae (Shand, 1997), the acuity of *N. brevirostris* larvae was relatively poor (2.98 cycles per degree). The overabundance of zooplankton in their habitat means that larval coral reef fishes can wander instead of using a lock-and-pursuit feeding behaviour i.e., they do not need to spot their food from a distance, but rather bump into it while floating in the plankton (Evans and Fernald, 1990; Fortier and Harris, 1989). Once settled on the reef, the visual acuity of *N. brevirostris* starts to increase in line with their growth (Fig. S2). Adult *N. brevirostris* were found to have a similar visual acuity (~11 cycles per degree) to other reef fishes of that size such as in the clown triggerfish, *Balistoides conspicillus*; a species that also inhabits the reef slope and shows a pronounced horizontal streak (Collin and Pettigrew, 1989).

Opsin gene evolution and expression

Phylogenetic reconstruction showed that the *N. brevirostris* visual opsins belong to the opsin gene clades usually found within percomorph fishes (Fig. 4). However, within the *RH2* genes, an exon-based phylogeny revealed that the *N. brevirostris RH2B* gene is likely to have undergone substantial gene conversion (Fig. 5A). As such, it occurs that parts of its first and second exon have been acquired from the *RH2A* paralog explaining its phylogenetic uncertainty when using whole coding region-based reconstructions (Fig. 4, Fig. S4). This is not that surprising, since *RH2* duplicates in teleosts are commonly found in tandem (e.g., Musilova et al., 2019) and, as is the case for other teleost opsin genes (Cortesi et al., 2015b; Hofmann and Carleton ,2009), frequently experience gene conversion (Cortesi et al., 2015b; Escobar-Camacho et al., 2016; Hofmann et al., 2012). This phenomenon is thought to be one of the main mechanism for concerted evolution in small gene families which often originate from tandem duplications (Li, 1997; Ohta, 1983) and could help to preserve gene function by

repairing null-mutations (Innan, 2009) or by resurrecting previously pseudogenized gene copies (Cortesi et al., 2015b). Since the *RH2* opsin genes are highly expressed in *N. brevirostris* they seem rather important for their visual ecology, and it is therefore likely that gene conversion played a major evolutionary role in maintaining their function.

Interestingly, the key spectral tuning site 122, despite being within the area of gene conversion, showed the RH2B specific 122Q (Fig. 5B,C). Since the remainder of the exon is almost identical to RH2A, it is likely that this site was re-gained post gene conversion suggesting that strong selection is maintaining two spectrally diverse RH2 copies in this species. As such, based on opsin gene expression, *N. brevirostris* could be behaviourally trichromatic (i.e., has three spectral sensitivities) for all three developmental stages, with the 'violet' *SWS2B*, and the 'blue-green' *RH2B* and *RH2A* genes being expressed in sufficient quantity to enable this level of chromatic analysis. Supporting these findings, microspectrophotometry (MSP) in adults of two closely related *Naso* species (*N. literatus* and *N. unicornis*; Sorenson et al., 2013) found three cone photoreceptors with spectral sensitivities ~ 420 nm λ_{max} for single cones, and ~ 490 nm λ_{max} and ~ 515 nm λ_{max} for the accessory and principle members of double cones, respectively (Losey et al., 2003). A short-shifted visual system with high-sensitivity in the violet to green range might benefit feeding on zooplankton and gelatinous prey during the larval and adult stages of *N. brevirostris* (Marshall et al., 2003). However, it seems at odds with the mainly algivorous diet of the juvenile stage, where a red-shifted visual system would be of advantage (Cortesi et al., 2018 preprint; Stieb et al., 2017).

Rather than the anticipated long-wavelength-shift in juveniles, the most notable change in opsin gene expression was found in the *RH2* copies between the larval and later *N. brevirostris* stages (Fig. 6A). A change in expression levels of *RH2B* and *RH2A* can also be found in coral reef damselfishes (Pomacentridae) (Stieb et al., 2016). On shallow, clear coral reefs a broad spectrum of light is available (Marshall et al., 2003). However, with increasing depth the long and short ends of the spectrum are cut off due to absorption and scattering through interfering particles, resulting in a blue mid-wavelength saturated light environment (Smith and Baker, 1981). Consequently, in an attempt to maximise photon catch, some damselfish species were found to increase the expression of the blue-sensitive *RH2B* gene and simultaneously decrease the expression of the green-sensitive *RH2A* gene with increasing depth (Stieb et al., 2016). In *N. brevirostris*, the shift in expression of *RH2* genes occurs between the larval and juvenile stages where depth differences do not seem that relevant. In lieu of depth, individuals migrate from a pelagic blue-shifted open water environment to the

more green-shifted light environment of the coral reef (Marshall et al., 2003). This could in theory explain the high *RH2A* expression in larval fish at the settlement stage, however, it does not explain the increase in *RH2B* expression post settlement (Fig. 6A). An increasing number of fishes are found to change their opsin gene expression to tune photoreceptors to the prevailing photic environment (e.g., Fuller et al., 2004; Härer et al., 2017; Hofmann et al., 2010; Luehrmann et al., 2018; Nandamuri et al., 2017; Shand et al., 2008; Stieb et al., 2016). At the opposite end of the spectrum, opsin gene expression might be pre-programmed either by phylogeny or on a species by species basis, as exemplified by only some damselfishes changing expression with depth (Stieb et al., 2016). It is therefore possible that opsin gene expression in *N. brevirostris* is under phylogenetic control and that changes in photic environment contribute very little to opsin gene expression in this case. Also, it is important to note that we currently not know if and how quantitative differences in opsin gene expression translate to the behaviour of *N. brevirostris*. Hence, until these results become available, it remains speculative as to what impact the changes observed here might have on the visual ecology of these fishes.

N. brevirostris was not found to express the UV-sensitive *SWS1* gene at any of the developmental stages. *SWS1* expression is often found in larval fishes and more generally in fishes feeding on zooplankton, with UV-vision thought to increase the detectability of this food source (Browman et al., 1994; Sabbah et al., 2010). Since *N. brevirostris* feeds on zooplankton at both larval and adult stages (Choat et al., 2002, 2004), the lack of *SWS1* expression seems striking. However, it does support ocular media measurements which revealed UV-blocking lenses in both larval and adult *N. brevirostris* (Siebeck and Marshall 2007). UV-blocking lenses seem common in many bigger coral reef fishes, which is thought to enhance sighting distance by reducing chromatic aberration and scatter, as well as protecting the eye from the damage caused by these high intensity wavelengths (Siebeck and Marshall, 2001). Instead, the expression of the violet sensitive *SWS2B* gene, since its spectral absorption curve reaches into the near-UV (based on MSP in closely related species; Losey et al., 2003), may be sufficient to increase the discrimination of zooplankton from the water background while foraging.

We furthermore found low expression of the *LWS* gene (<6%) at all developmental stages. This suggests that *LWS* expression is either restricted to certain areas of the retina, interspersed at low frequency across the retina, or some photoreceptors might co-express *LWS* with an *RH2* gene (e.g., Cortesi et al., 2016; Dalton et al., 2014; Torres-Dowdall et al., 2017). MSP in related *Naso* species did not show any long-wavelength-sensitive

photoreceptors, nor did it show any evidence for opsin co-expression (i.e., red-shifted unusually broad absorbance peaks; Losey et al., 2003). Since this technique only samples as subset of the photoreceptors across the retina, it might be that the photoreceptors containing this pigment were missed due to their low number or that *LWS* was simply not expressed in these fishes.

It is possible that the *LWS* expression found here is just a by-product of the way opsin gene expression is controlled and that it does not serve any ecological function. Nevertheless, *LWS* expression did increase steadily with development (Fig. 6A). Hence, an alternative explanation might be that *LWS* is co-expressed with an *RH2* gene, which has been shown to increase achromatic discrimination in cichlids (Dalton et al., 2014). Moreover, *LWS* expression has recently been shown to be correlated to algal feeding in damselfishes (Stieb et al., 2017), and blennies (Cortesi et al., 2018 preprint). Since *N. brevirostris* juveniles and to a certain extend also adults (Choat et al., 2002), feed on algal turf, an increase in *LWS* expression in later stages, may improve feeding efficiency due to the increased contrast of algae against the reef background (Marshall et al., 2003; Stieb et al., 2017). In situ hybridisation studies (e.g., Dalton et al., 2014, 2016; Stieb et al., in press; Torres-Dowdall et al., 2017) coupled with behavioural colour-vision experiments (e.g., Cheney et al., 2019) will be needed in the future to assess the distribution and function of the various opsin genes and ultimately the colour vision system of *N. brevirostris*.

Conclusion

Using a multidisciplinary approach, we analysed the ontogeny of the visual system of *N. brevirostris*. Changes in retinal topographies and opsin gene expression were mainly found between the larval and juvenile stages, with few minor modifications thereafter. The juvenile stage in particular did not seem to match its ecology very well, which may be explained by the short duration of this stage compared to the lifespan of these fishes. This is different to the steady development that was found in other reef fishes (Cortesi et al., 2016; Shand et al., 2008; Suresh and Julia, 2001) and highlights the need for a comprehensive analysis of visual ontogeny across the reef fish community.

Acknowledgements

We would like to thank Sara M. Stieb, Vivien Rothenberger, Simon Dunn, and the staff of Tetiaroa Society (Moana LeRohellec) and of CRIOBE (Camille Gache) for assistance with specimen collection. We furthermore thank the staff at the Lizard Island Research Station for logistical support, and Janette Edson from the Queensland Brain Institute's (QBI) sequencing facility for library preparation and RNA sequencing. We also acknowledge QBI's Advanced Microscopy Facility for the use of the Stereo Investigator (software v. 2017.01.1), generously supported by the Australian Government through the ARC LIEF grant LE100100074.

Competing interests

The authors declare no competing interests.

Author contributions

F. C. conceived the study and designed the experiments together with F.d.B and N.J.M. V.T., F.d.B and F.C. performed the experiments and analysed the data. All authors contributed to specimen collection. V.T. wrote the initial draft of the manuscript and all authors agreed to the final version of the manuscript.

Funding

This study was funded by the Sea World Research & Rescue Foundation Inc., an Australian Research Council Discovery Project Grant (ARC DP180102363), and by the Tetiaroa Society, the Leonardo Di Caprio Foundation and Mission Blue for the CRIOBE study at Tetiaroa. F.d.B. was supported by an ARC DECRA Fellowship (DE180100949), N.J.M. by an ARC Laureate Fellowship, and F.C. by a UQ Development Fellowship.

Data availability

Raw-read transcriptomes (PRJNA590573; SAMN13340708- 13340719) and single gene sequences (MN720499-MN720503) are available through GenBank (https://www.ncbi.nlm.nih.gov/genbank/). Gene alignments, phylogenies, transcriptome assemblies, and retinal topography maps of single and double cones for each individual can be accessed through Dryad (doi:10.5061/dryad.k6djh9w37). All other data is given either in the main manuscript or the supplementary material.

List of abbreviations

bp	base pairs
cds	coding sequence
CE	Shaeffer's coefficient of error
DC	double cones
LWS	long-wavelength-sensitive
LWS	long-wavelength-sensitive opsin gene
MSP	microspectrophotometry
MWS	mid-wavelength sensitive
PDG	peak density of ganglion cells
RH1	rhodopsin 1 opsin gene
RH2A, RH2B	rhodopsin like 2 opsin genes
SC	single cones
SL	standard length
SNP	single nucleotide polymorphism
SRP	spatial resolving power
SWS	short-wavelength-sensitive
SWS1	short-wavelength-sensitive 1 opsin gene
SWS2	short-wavelength-sensitive 2 opsin gene
λ_{max}	peak spectral sensitivity

References

Afgan, E., Sloggett, C., Goonasekera, N., Makunin, I., Benson, D., Crowe, M., Gladman, S., Kowsar, Y., Pheasant, M., Horst, R. and Lonie, A. (2015). Genomics Virtual Laboratory: A practical bioinformatics workbench for the Cloud. *PLOS ONE.* **10**, e0140829.

Baddeley, A. and Turner, R. (2005). Spatstat: an R package for analyzing spatial point patterns. *J. Stat. Softw.* **12,** 1-42.

Bailes, H. J., Trezise, A. E. and Collin, S. P. (2006). The number, morphology, and distribution of retinal ganglion cells and optic axons in the Australian lungfish *Neoceratodus forsteri* (Krefft 1870). *Vis. Neurosci.* **23**, 257-273.

Barnes, R. S. K. and Hughes, R. N. (1999). *An introduction to marine ecology.* Oxford, UK: Blackwell Science Ltd, a Blackwell Publishing company.

Besson, M., Gache, C., Brooker, R. M., Moussa, R. M., Waqalevu, V. P., LeRohellec, M., Jaouen, V., Peyrusse, K., Berthe, C., Bertucci, F. et al. (2017). Consistency in the supply of larval fishes among coral reefs in French Polynesia. *PLOS ONE.* **12**, e0178795.

Boehlert, G. W. (1996). Larval dispersal and survival in tropical reef fishes. In *Reef Fisheries* (ed. N. V. C. Polunin and C. M. Roberts), pp. 61-84. Dordrecht, NL: Springer Netherlands.

Bolger, A. M., Lohse, M. and Usadel, B. (2014). Trimmomatic: a flexible trimmer for Illumina sequence data. *Bioinformatics.* **30**, 2114-2120.

Bowmaker, J. K. (2008). Evolution of vertebrate visual pigments. *Vision Res.* **48**, 2022-2041.

Bowmaker, J. K. and Kunz, Y.W. (1987). Ultraviolet receptors, tetrachromatic colour vision and retinal mosaics in the brown trout (*Salmo trutta*): age-dependent changes. *Vision Res.* **27**, 2101-2108.

Bozzano, A. and Collin, S. P. (2000). Retinal ganglion cell topography in elasmobranchs. *Brain Behav. Evol.* **55**, 191-208.

Brandl, S. J. and Bellwood, D. R. (2013). Morphology, sociality, and ecology: can morphology predict pairing behavior in coral reef fishes? *Coral Reefs.* **32**, 835-846.

Browman, H. I., Novales-Flamarique, I. and Hawryshyn, C. (1994). Ultraviolet photoreception contributes to prey search behaviour in two species of zooplanktivorous fishes. *J. Exp. Biol.* **186**, 187-198.

Carleton, K. L., Spady, T. C., Streelman, J. T., Kidd, M. R., McFarland, W. N. and Loew, E. R. (2008). Visual sensitivities tuned by heterochronic shifts in opsin gene expression. *BMC Biol.* **6**, 22.

Caves, E. M., Sutton, T. T. and Johnsen, S. (2017). Visual acuity in ray-finned fishes correlates with eye size and habitat. *J. Exp. Biol.* **220**, 1586-1596.

Cheney, K. L., Green, N. F., Vibert, A. P., Vorobyev, M., Marshall, N. J., Osorio, D. C. and Endler, J. A. (2019). An Ishihara-style test of animal colour vision. *J. Exp. Biol.* **222**, jeb189787.

Chinen A, Matsumoto Y, Kawamura S. (2005). Reconstitution of ancestral green visual pigments of zebrafish and molecular mechanism of their spectral differentiation. Molecular biology and evolution. *Mol. Biol. Evol.* **22**, 1001-1010.

Choat, J. H. and Axe, L. M. J. (1996). Growth and longevity in acanthurid fishes; an analysis of otolith increments. *Mar. Ecol. Prog. Ser.* **134**, 15-26.

Choat, J. H., Clements, K. D. and Robbins, W. D. (2002). The trophic status of herbivorous fishes on coral reefs. I. Dietary analyses. *Mar. Biol.* **140**, 613-623.

Choat, J. H., Robbins, W. D. and Clements, K. D. (2004). The trophic status of herbivorous fishes on coral reefs. II. Food processing modes and trophodynamics. *Mar. Biol.* **145**, 445-454.

Coimbra, J. P., Marceliano, M. L., da Silveira Andrade-Da-Costa, B. L. and Yamada, E. S. (2006). The retina of tyrant flycatchers: topographic organization of neuronal density and size in the ganglion cell layer of the great kiskadee *Pitangus sulphuratus* and the rusty margined flycatcher *Myiozetetes cayanensis* (Aves: Tyrannidae). *Brain Behav. Evol.* **68**, 15-25.

Coimbra, J. P., Trévia, N., Videira Marceliano, M. L., da Silveira Andrade-Da-Costa, B. L., Picanço-Diniz, C. W. and Yamada, E. S. (2009). Number and distribution of neurons in the retinal ganglion cell layer in relation to foraging behaviors of tyrant flycatchers. *J. Comp. Neurol.* **514**, 66-73.

Coimbra, J. P., Nolan, P. M., Collin, S. P. and Hart, N. S. (2012). Retinal ganglion cell topography and spatial resolving power in penguins. *Brain Behav. Evol.* **80**, 254-268.

Collin, S. P. (1988). The retina of the shovel-nosed ray, *Rhinobatos batillum* (Rhinobatidae): morphology and quantitative analysis of the ganglion, amacrine and bipolar cell populations. *Exp. Biol.* **47**, 195-207.

Collin, S. P. (2008). A web-based archive for topographic maps of retinal cell distribution in vertebrates. *Clin. Exp. Optom.* **91**, 85-95.

Collin, S. P. and Pettigrew, J. D. (1988a). Retinal topography in reef teleosts. I. Some species with well-developed areae but poorly-developed streaks. *Brain Behav. Evol.* **31**, 269-282.

Collin, S. P. and Pettigrew, J. D. (1988b). Retinal topography in reef teleosts. II. Some species with prominent horizontal streaks and high-density areae. *Brain Behav. Evol.* **31**, 283-295.

Collin, S. P. and Pettigrew, J. D. (1988c). Retinal ganglion cell topography in teleosts: a comparison between nissl-stained material and retrograde labelling from the optic nerve. *J. Comp. Neurol.* **276**, 412-422.

Collin, S. P. and Pettigrew, J. D. (1989). Quantitative comparison of the limits on visual spatial resolution set by the ganglion cell layer in twelve species of reef teleosts. *Brain Behav. Evol.* **34**, 184-192.

Collin, S. P. and Shand, J. (2003). Retinal sampling and the visual field in fishes. in *Sensory Processing in Aquatic Environments* (ed. S. P. Collin and N. J. Marshall), pp. 139-169. New York, NY: Springer New York.

Cortesi, F., Feeney, W. E., Ferrari, M. C., Waldie, P. A., Phillips, G. A., McClure, E. C., Sköld, H. N., Salzburger, W., Marshall, N. J. and Cheney, K. L. (2015a). Phenotypic plasticity confers multiple fitness benefits to a mimic. *Curr. Biol.* **25**, 949-954.

Cortesi, F., Musilová, Z., Stieb, S. M., Hart, N. S., Siebeck, U. E., Cheney, K. L., Salzburger, W. and Marshall, N. J. (2016). From crypsis to mimicry: changes in colour and the configuration of the visual system during ontogenetic habitat transitions in a coral reef fish. *J. Exp. Biol.* **219**, 2545-2558.

Cortesi, F., Cheney, K. L., Cooke, G. M. and Ord, T. (2018). Opsin gene evolution in amphibious and terrestrial combtooth blennies (Blenniidae). *bioRxiv* doi:10.1101/503516.

Cortesi, F., Musilová, Z., Stieb, S. M., Hart, N. S., Siebeck, U. E., Malmstrøm, M., Tørresen, O. K., Jentoft, S., Cheney, K. L., Marshall, N. J. et al. (2015b). Ancestral duplications and highly dynamic opsin gene evolution in percomorph fishes. *Proc. Natl. Acad. Sci. U.S.A.* **112**, 1493-1498.

Cronin, T. W., Johnsen, S., Marshall, N. J. and Warrant, E. J. (2014). *Visual ecology*. Princeton, NJ: Princeton University Press.

Dalton, B. E., de Busserolles, F., Marshall, N. J. and Carleton, K. L. (2016). Retinal specialization through spatially varying cell densities and opsin coexpression in cichlid fish. *J. Exp. Biol.* **220**, 266-277.

Dalton, B. E., Loew, E. R., Cronin, T. W. and Carleton, K. L. (2014). Spectral tuning by opsin coexpression in retinal regions that view different parts of the visual field. *Proc. R. Soc. B Biol. Sci.* **281**, 20141980.

Darriba, D., Taboada, G. L., Doallo, R. and Posada, D. (2012). jModelTest 2: more models, new heuristics and parallel computing. *Nat. Methods* **9**, 772.

de Busserolles, F., Marshall, N. J. and Collin, S. P. (2014a). Retinal ganglion cell distribution and spatial resolving power in deep-sea lanternfishes (Myctophidae). *Brain Behav. Evol.* **84**, 262-276.

de Busserolles, F., Fitzpatrick, J. L., Marshall, N. J. and Collin, S. P. (2014b). The influence of photoreceptor size and distribution on optical sensitivity in the eyes of lanternfishes (Myctophidae). *PLOS ONE* **9**, e99957.

de Busserolles, F., Cortesi, F., Helvik, J. V., Davies, W. I. L., Templin, R. M., Sullivan, R. K. P., Michell, C. T., Mountford, J. K., Collin, J. K., Irigoien, X. et al. (2017). Pushing the limits of photoreception in twilight conditions: the rod-like cone retina of the deep-sea pearlsides. *Sci. Adv.* **3**, eaao4709.

Endler, J. A. (1990). On the measurement and classification of colour in studies of animal colour patterns. *Biol. J. Linn. Soc.* **41**, 315-352.

Escobar-Camacho, D., Ramos, E., Martins, C. and Carleton, K. L. (2016). The opsin genes of amazonian cichlids. *Mol. Ecol.* **26**, 1343-1356.

Evans, B. I. and Fernald, R. D. (1990). Metamorphosis and fish vision. *J. Neurobiol.* **21**, 1037-1052.

Fernald, R. D. (1988). Aquatic adaptations in fish eyes. In *Sensory Biology of Aquatic Animals* (ed. J. Atema, R. R. Fay, A. N. Popper and W. N. Tavolga), pp. 435-466. New York, NY: Springer New York.

Fortier, L. and Harris, R. P. (1989). Optimal foraging and density-dependent competition in marine fish larvae. *Mar. Ecol. Prog. Ser.* **51**, 19-33.

Fritsch, R., Collin, S. P. and Michiels, N. K. (2017). Anatomical analysis of the retinal specializations to a crypto-benthic, micro-predatory lifestyle in the Mediterranean triplefin blenny *Tripterygion delaisi*. *Front. Neuroanat.* **11**, 122.

Fritsches, K. A., Marshall, N. J. and Warrant, E. (2003). Retinal specializations in the blue marlin: eyes designed for sensitivity to low light levels. *Mar. Freshw. Res.* **54**, 333-341.

Fuller, R. C., Carleton, K. L., Fadool, J. M., Spady, T. C. and Travis, J. (2004). Population variation in opsin expression in the bluefin killifish, *Lucania goodei*: a real-time PCR study. *J. Comp. Physiol. A* **190**, 147-154.

Garza-Gisholt, E., Hemmi, J. M., Hart, N. S. and Collin, S. P. (2014). A comparison of spatial analysis methods for the construction of topographic maps of retinal cell density. *PLOS ONE* **9**, e93485.

Glaser, E. M. and Wilson, P. D. (1998). The coefficient of error of optical fractionator population size estimates: a computer simulation comparing three estimators. *J. Microsc.* **192**, 163-171.

Haas, B. J., Papanicolaou, A., Yassour, M., Grabherr, M., Blood, P. D., Bowden, J., Couger, M. B., Eccles, D., Li, B. and Lieber, M. (2013). De novo transcript sequence reconstruction from RNA-seq using the Trinity platform for reference generation and analysis. *Nat. Protoc.* **8**, 1494.

Härer, A., Torres-Dowdall, J. and Meyer, A. (2017). Rapid adaptation to a novel light environment: the importance of ontogeny and phenotypic plasticity in shaping the visual system of Nicaraguan Midas cichlid fish (*Amphilophus citrinellus* spp.). *Mol. Ecol.* **26**, 5582-5593.

Helfman, G., Collette, B. B., Facey, D. E. and Bowen, B. W. (2009). *The diversity of fishes: biology, evolution, and ecology*. West Sussex, UK: Wiley-Blackwell.

Hofmann, C. M. and Carleton, K. L. (2009). Gene duplication and differential gene expression play an important role in the diversification of visual pigments in fish. *Integr. Comp. Biol.* **49**, 630-643.

Hofmann, C. M., O'Quin, K. E. , Smith, A. R. and Carleton, K. L. (2010). Plasticity of opsin gene expression in cichlids from Lake Malawi. *Mol. Ecol.* **19**, 2064-2074.

Hofmann, C. M., Marshall, N. J., Abdilleh, K., Patel, Z., Siebeck, U. E. and Carleton, K. L. (2012). Opsin evolution in damselfish: convergence, reversal, and parallel evolution across tuning sites. *J. Mol. Evol.* **75**, 79-91.

Holzer, G., Besson, M., Lambert, A., Francois, L., Barth, P., Gillet, B., Hughes, S., Piganeau, G., Leulier, F., Viriot, L. et al. (2017). Fish larval recruitment to reefs is a thyroid hormone-mediated metamorphosis sensitive to the pesticide chlorpyrifos. *eLife* **6**, e27595.

Hughes, A. (1975). A quantitative analysis of the cat retinal ganglion cell topography. *J. Comp. Neurol.* **163**, 107-128.

Hughes, A. (1977). The topography of vision in mammals of contrasting life style: comparative optics and retinal organisation. In *The visual system in vertebrates* (ed. F. Crescitelli), pp. 613-756. Berlin, DE: Springer Berlin Heidelberg.

Hunt, D. M., Hankins, M. W., Collin S. P. and Marshall, N. J. (2014). *Evolution of visual and non-visual pigments*. New York, NY: Springer New York.

Innan, H. (2009). Population genetic models of duplicated genes. *Genetica* **137**, 19.

Ito, H. and Murakami, T. (1984). Retinal ganglion cells in two teleost species, *Sebastiscus marmoratus* and *Navodon modestus. J. Comp. Neurol.* **229**, 80-96.

Job, S. D. and Bellwood, D. R. (2000). Light sensitivity in larval fishes: implications for vertical zonation in the pelagic zone. *Limnol. Oceanogr.* **45**, 362-371.

Katoh, K. and Standley, D. M. (2013). MAFFT multiple sequence alignment software version 7: improvements in performance and usability. *Mol. Biol. Evol.* **30**,772-780.

Wong, R. O. L. and Hughes, A. (1987). Developing neuronal populations of the cat retinal ganglion cell layer. *J. Comp. Neurol.* **262**, 473-495.

Lasiak, T.A. (1986). Juveniles, food and the surf zone habitat: implications for teleost nursery areas. *South African Journal of Zoology* **21**,51-56.

Lecchini, D., Dufour, V., Carleton, J., Strand, S. and Galzin, R. (2004). Estimating the patch size of larval fishes during colonization on coral reefs. *J. Fish Biol.* **65**, 1142-1146.

Lecchini, D., Planes, S. and Galzin R. (2005a). Experimental assessment of sensory modalities of coral-reef fish larvae in the recognition of their settlement habitat. *Behav. Ecol. Sociobiol*. **58**, 18-26.

Lecchini, D., Shima, J., Banaigs, B. and Galzin, R. (2005b). Larval sensory abilities and mechanisms of habitat selection of a coral reef fish during settlement. *Oecologia* **143**, 326-334.

Leis, J. M. and Carson-Ewart, B. M. (1999). In situ swimming and settlement behaviour of larvae of an Indo-Pacific coral-reef fish, the coral trout *Plectropomus leopardus* (Pisces: Serranidae). *Mar. Biol.* **134**, 51-64.

Lin, J. J., Wang, F. Y., Li, W. H. and Wang, T. Y. (2017). The rises and falls of opsin genes in 59 ray-finned fish genomes and their implications for environmental adaptation. *Sci. Rep.* **7**, 15568.

Lisney, T. J. and Collin, S. P. (2008). Retinal ganglion cell distribution and spatial resolving power in elasmobranchs. *Brain Behav. Evol.* **72**, 59-77.

Loew, E. R., McFarland, W. N., Mills E. L. and Hunter, D. (1993). A chromatic action spectrum for planktonic predation by juvenile yellow perch, *Perca flavescens*. Can. J. Zool. **71**, 384-386.

Losey, G. S., McFarland, W. N., Loew, E. R., Zamzow, J. P., Nelson, P. A. and Marshall, N. J. (2003). Visual biology of Hawaiian coral reef fishes. I. Ocular transmission and visual pigments. *Copeia* **2003**, 433-454.

Luehrmann, M., Stieb, S M., Carleton, K. L., Pietzker, A., Cheney, K. L. and Marshall, N. J. (2018). Short-term colour vision plasticity on the reef: changes in opsin expression under varying light conditions differ between ecologically distinct fish species. *J. Exp. Biol.* **221**, jeb175281.

Lythgoe, J. N. (1979). *Ecology of vision.* New York, US: Oxford University Press.

Marshall, N. J., Jennings, K., McFarland W. N., Loew, E. R. and Losey, G. S. (2003). Visual biology of Hawaiian coral reef fishes. III. Environmental light and an integrated approach to the ecology of reef fish vision. *Copeia* **2003**, 467-480.

Matthiessen, L. (1882). Ueber die Beziehungen, welche zwischen dem Brechungsindex des Kerncentrums der Krystalllinse und den Dimensionen des Auges bestehen. *Archiv für die gesamte Physiologie des Menschen und der Tiere* **27**, 510-523.

McComb, D. M., Tricas, T. C. and Kajiura, S. M. (2009). Enhanced visual fields in hammerhead sharks. *J. Exp. Biol.* **212**, 4010-4018.

Miller, M. A., Pfeiffer, W. and Schwartz, T. (2010). Creating the CIPRES Science Gateway for inference of large phylogenetic trees. Gateway Computing Environments Workshop (GCE), IEEE, 1-8.

Mouritsen, H., Atema, J., Kingsford, M. J. and Gerlach, G. (2013). Sun compass orientation helps coral reef fish larvae return to their natal reef. *PLOS ONE* **8**, e66039.

Mundy, B. C. (2005). Checklist of the fishes of the Hawaiian Archipelago. *Bishop Mus. Bull. Zool.* **6**, 1-704.

Musilova, Z., Cortesi, F., Matschiner, M., Davies, W. I. L., Patel, J. S., Stieb, S. M., de Busserolles, F., Malmstrøm, M., Tørresen, O. K., Brown, C. J. et al. (2019). Vision using multiple distinct rod opsins in deep-sea fishes. *Science* **364**, 588-592.

Nandamuri, S. P., Yourick, M. R. and Carleton, K. L. (2017). Adult plasticity in African cichlids: rapid changes in opsin expression in response to environmental light differences. *Mol. Ecol.* **26**, 6036-6052.

Novales-Flamarique, I. (2016). Diminished foraging performance of a mutant zebrafish with reduced population of ultraviolet cones. *Proc. R. Soc. B Biol. Sci.* **283**, 20160058.

Peichl, L., Nemec, P. and Burda, H. (2004). Unusual cone and rod properties in subterranean African mole-rats (Rodentia, Bathyergidae). *Eur. J. Neurosci*. **19**, 1545-1558.

Purcell, S. W. and Bellwood, D. R. (1993). A functional analysis of food procurement in two surgeonfish species, *Acanthurus nigrofuscus* and *Ctenochaetus striatus* (Acanthuridae). *Environ. Biol. Fishes*, **37**, 139-159.

Randall, J. E., Gerald, R. A. and Steene, R. C. (1997). *Fishes of the great barrier reef and coral sea*. Honolulu, USA: University of Hawaii Press.

Ronquist, F., Teslenko, M., Van Der Mark, P., Ayres, D. L., Darling, A., Höhna, S., Larget, B., Liu, L., Suchard, M. A. and Huelsenbeck, J. P. (2012). MrBayes 3.2: efficient Bayesian phylogenetic inference and model choice across a large model space. *Syst. Biol.* **61**, 539-542.

Sabbah, Shai, Raico Lamela Laria, Suzanne M. Gray, and Craig W. Hawryshyn. (2010). Functional diversity in the color vision of cichlid fishes. *BMC Biol*. **8**, 133.

Sale, Peter F. (2013). *The ecology of fishes on coral reefs*. Elsevier).

Schindelin, J., I. Arganda-Carreras, E. Frise, V. Kaynig, M. Longair, T. Pietzsch, S. Preibisch, C. Rueden, S. Saalfeld, B. Schmid, J. Y. Tinevez, D. J. White, V. Hartenstein, K. Eliceiri, P. Tomancak, and A. Cardona. (2012). Fiji: an open-source platform for biological-image analysis. *Nat Methods*. **9**, 676-82.

Shand, Julia. (1997). Ontogenetic changes in retinal structure and visual acuity: a comparative study of coral-reef teleosts with differing post-settlement lifestyles. *Environ. Biol. Fishes*. **49**, 307-22.

Shand, Julia, Michael A Archer, and Shaun P Collin. (1999). Ontogenetic changes in the retinal photoreceptor mosaic in a fish, the black bream, *Acanthopagrus butcheri*. *J. Comp. Neurol*. **412**, 203-17.

Shand, Julia, Stephanie M Chin, Alison M Harman, Stephen Moore, and Shaun P Collin. (2000). Variability in the location of the retinal ganglion cell area centralis is correlated with ontogenetic changes in feeding behavior in the black bream, *Acanthopagrus butcheri* (Sparidae, Teleostei). *Brain Behav. Evol*. **55**, 176-90.

Shand, Julia, Wayne L Davies, Nicole Thomas, Lois Balmer, Jill A Cowing, Marie Pointer, Livia S Carvalho, Ann EO Trezise, Shaun P Collin, and Lyn D Beazley. (2008). The influence of ontogeny and light environment on the expression of visual pigment opsins in the retina of the black bream, *Acanthopagrus butcheri*. *J. Exp. Biol*. **211**, 1495-503.

Siebeck, U. E., and N. J. Marshall. (2007). Potential ultraviolet vision in pre-settlement larvae and settled reef fish—A comparison across 23 families. *Vision Research*. **47**, 2337-52.

Siebeck, Ulrike E., and N. Justin Marshall. (2001). Ocular media transmission of coral reef fish — can coral reef fish see ultraviolet light? *Vision Res*. **41**, 133-49.

Slomianka, L, and Mark J West. (2005). Estimators of the precision of stereological estimates: an example based on the CA1 pyramidal cell layer of rats. *Neuroscience*. **136**, 757-67.

Smith, Raymond C., and Karen S. Baker. (1981). Optical properties of the clearest natural waters (200–800 nm). *Appl Opt*. **20**, 177-84.

Sorenson, L., Francesco Santini, Giorgio Carnevale, and Michael E. Alfaro. (2013). A multi-locus timetree of surgeonfishes (Acanthuridae, Percomorpha), with revised family taxonomy. *Mol. Phylogenet. Evol*. **68**, 150-60.

Spady, Tyrone C., Juliet W. L. Parry, Phyllis R. Robinson, David M. Hunt, James K. Bowmaker, and Karen L. Carleton. 2006. Evolution of the cichlid visual palette through ontogenetic subfunctionalization of the opsin gene arrays. *Mol. Biol. Evol*. **23**, 1538-47.

Stieb, Sara M, Karen L Carleton, Fabio Cortesi, N Justin Marshall, and Walter Salzburger. (2016). Depth-dependent plasticity in opsin gene expression varies between damselfish (Pomacentridae) species. *Mol. Ecol*. **25**, 3645-61.

Stieb, Sara M., Fabio Cortesi, Lorenz Sueess, Karen L. Carleton, Walter Salzburger, and N. J. Marshall. (2017). Why UV vision and red vision are important for damselfish (Pomacentridae): structural and expression variation in opsin genes. *Mol. Ecol*. **26**, 1323-42.

Stieb, Sara M., Fanny de Busserolles, Karen L. Carleton, Fabio Cortesi, Wen-Sung Chung, Brian Dalton, Luke A. Hammond, and Justin Marshall. (2019). Seeing through the eyes of the anemonefish, *Amphiprion akindynos*: a detailed investigation of its visual system and visual ecology. *In review*.

Stone, Jonathan, and Elizabeth Johnston. (1981). The topography of primate retina: a study of the human, bushbaby, and new-and old-world monkeys. *J. Comp. Neurol*. **196**, 205-23.

Suresh, D. Job, and Shand Julia. (2001). Spectral sensitivity of larval and juvenile coral reef fishes: implications for feeding in a variable light environment. *Mar. Ecol. Prog. Ser*. **214**, 267-77.

Torres-Dowdall, J., Michele E. R. Pierotti, Andreas Härer, Nidal Karagic, Joost M. Woltering, Frederico Henning, Kathryn R. Elmer, and Axel Meyer. (2017). Rapid and parallel adaptive evolution of the visual system of Neotropical Midas cichlid fishes. *Mol. Biol. Evol*. **34**, 2469-2485.

Ullmann, J. F., B. A. Moore, S. E. Temple, E. Fernandez-Juricic, and S. P. Collin. (2012). The retinal wholemount technique: a window to understanding the brain and behaviour. *Brain Behav. Evol*. **79**, 26-44.

Walls, G. L. (1934). The Reptilian Retina: I. A new concept of visual-cell evolution. *Am. J. Ophthalmol*. **17**, 892-915.

Walls, Gordon Lynn. (1942). The vertebrate eye and its adaptive radiation. Bloomfield Hills, Michigan, USA: The Cranbrook Press.

West, M. J., L. H. J. G. Slomianka, and H. J. G. Gundersen. (1991). Unbiased stereological estimation of the total number of neurons in the subdivisions of the rat hippocampus using the optical fractionator. *Anat. Rec*. **231**, 482-97.

Tables

Table 1 Summary of ganglion cell quantitative data obtained using the optical fractionator method on the wholemounted retinas of three developmental stages of *N. brevirostris*.

Stage	Individual	SL (cm)	Peak cell density, (cells/mm^2)	Mean cell density (cells/mm^2)	Total cells	Lens ∅ (mm)	SRP
Adult	ID1	30.6	20,617	5,340	2,034,000	6.6	10.6
	ID2	30.8	20,370	4,772	2,100,825	6.9	11.0
Juvenile	ID1	13.8	23,750	8,130	1,617,968	4.7	8.1
	ID2	15.2	24,531	8,688	1,737,656	4.9	8.6
	ID3	15.7	21,875	8,584	1,450,625	4.5	7.5
Larvae	ID1	3.18	30,400	19,439	208,975	1.4	2.98

SL = standard length, SRP = spatial resolving power, ∅ = diameter

Table 2 Summary of photoreceptor quantitative data obtained using the optical fractionator method on the wholemounted retinas of three developmental stages of *N. brevirostris*.

Stage	Individual	SL (cm)	Total DC	Peak DC (cells/mm^2)	Total SC	Peak SC (cells /mm^2)	Total cones	Peak TC (cells mm^2)
Adult	ID3	29.7	3,738,296	23,703	1,926,513	12,098	5,664,809	35,801
	ID4	27.7	3,820,839	21,208	1,972,975	12,345	5,793,814	33,553
Juvenile	ID3	13.8	2,466,222	34,218	1,283,524	18,125	3,749,746	52,343
	ID4	18.5	3,212,099	32,968	1,667,475	17,187	4,879,574	50,155
Larvae	ID2	3.08	452,010	45,432	231,371	23,703	683,381	69,135
	ID3	3.30	413,476	45,432	211,105	23,704	624,581	69,136

SL = standard length, DC = double cones; SC = single cones

Figures

Fig. 1 *Naso brevirostris* developmental stages. The spotted unicornfish**,** *N. brevirostris*, shows pronounced ontogenetic changes in habitat, diet and morphology. (A) A 'transparent' zooplanktivorous larva at the settlement stage (i.e., when returning from the pelagic to the reef). (B) An algivorous juvenile that lives in close proximity to the reef. (C) A zooplanktivorous adult that lives in the water column above the reef. Note the growth of the prominent snout throughout development.

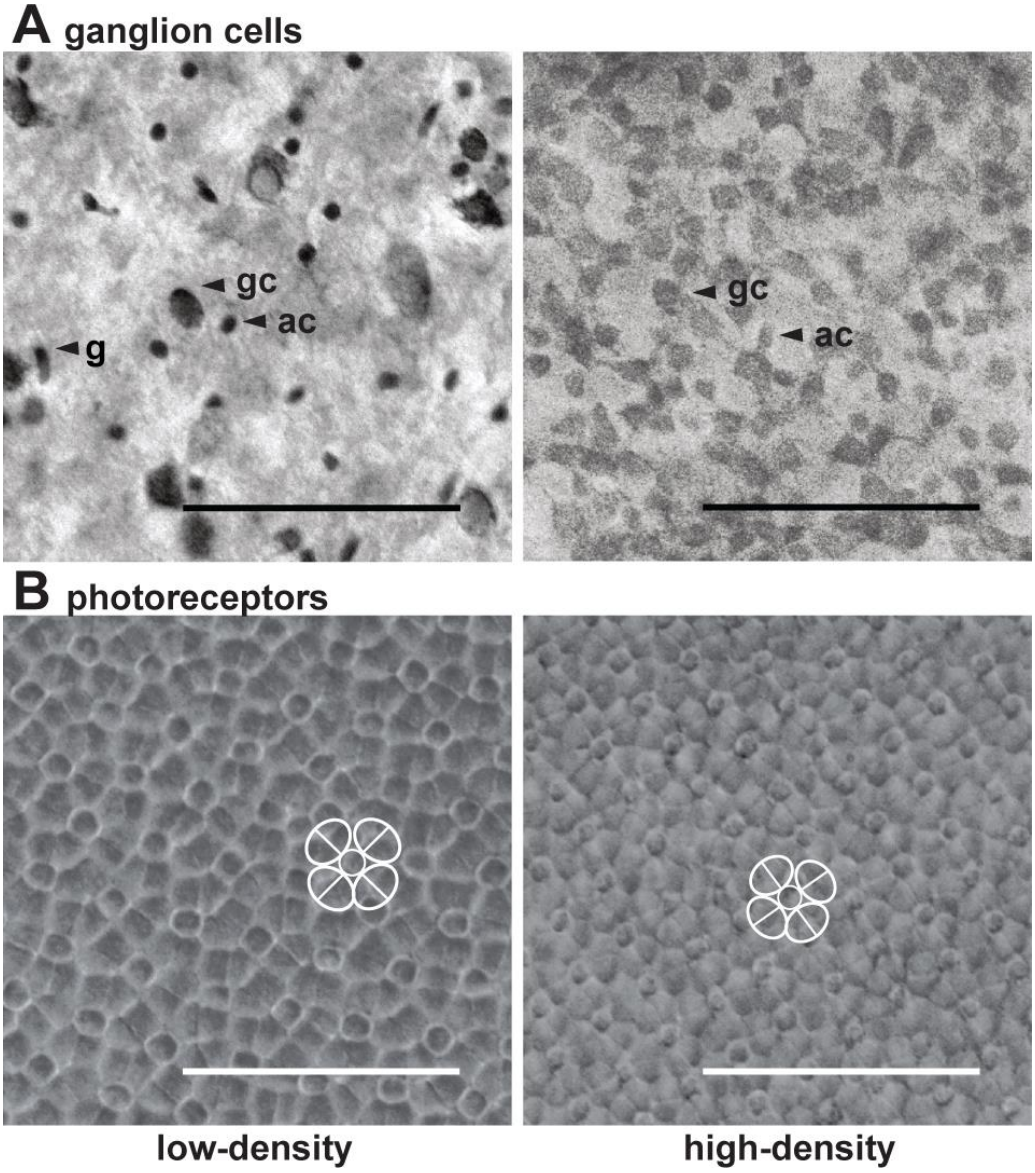

Fig. 2 Light micrographs of various retinal layers as found in an adult *N. brevirostris*. (A) Micrographs of the Nissl-stained ganglion cell layer taken in a low-density (nasal part) and a peak-density area (central part) of the retina. Ganglion cells (gc) could clearly be distinguished from glial cells (g) by their round shape and difference in size. Distinguishing amacrine cells (ac) from gc, however, was more difficult. (B) Micrographs of the photoreceptor layer taken in a low-density (nasal part) and a peak-density area (temporal part). Photoreceptors formed a square mosaic with a central single cone (sc) surrounded by four double cones (dc). Scale bar = 50 μm.

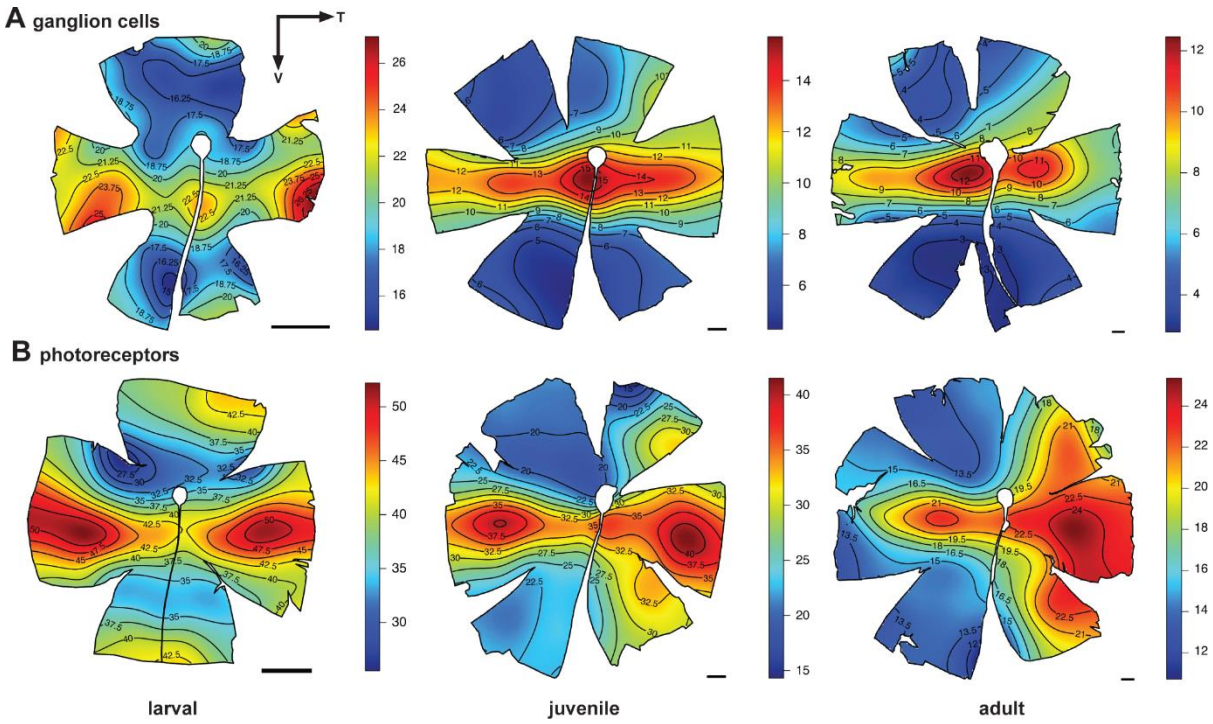

Fig. 3 Topographic heat maps of ganglion and photoreceptor-cell distribution. (A) Topographic distribution of retinal ganglion cells revealed a pronounced horizontal streak with a peak cell density in the central area in adult and juvenile individuals. In the larvae, the streak was less pronounced and peak cell densities were found in the nasal and temporal parts instead (see Fig. S1 for maps of additional individuals). (B) Topographic distribution of total photoreceptors (double and single cones) revealed an increase in specialization with life stage from a weak horizontal streak with two large areas of high cell densities in larvae to the formation of a pronounced horizontal streak and a weak dorsal vertical streak in juveniles. A more pronounced dorsal vertical streak was found in adults (see Fig S2 and the Dryad repository for single and double cone maps as well as maps of additional individuals). Black lines represent isodensity contours, and values are expressed in densities $x10^3$ cells/mm^2. V = Ventral, T = temporal. Scale bar = 1 mm.

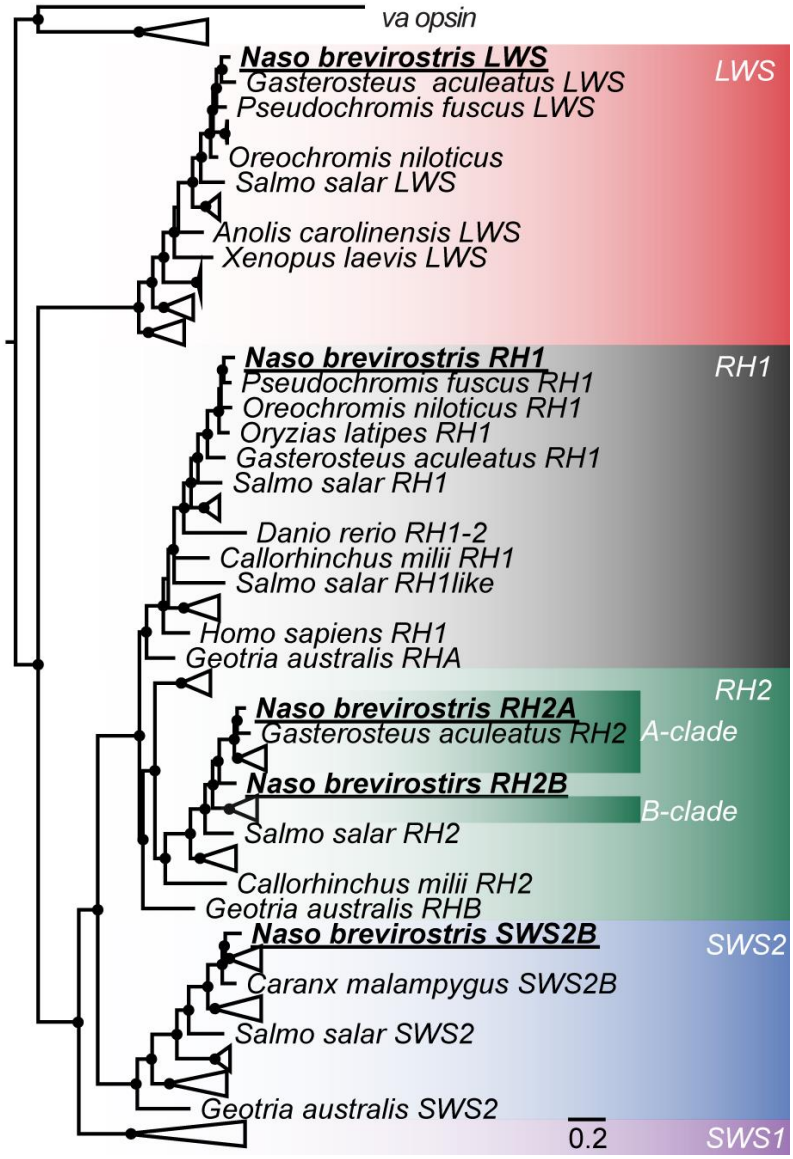

Fig. 4 Vertebrate visual opsin gene phylogeny. The different *N. brevirostris* opsin genes which were mined from the retinal transcriptomes are highlighted in bold and belong to four of the five major visual opsin classes. Black spheres indicate Bayesian posterior probabilities > 0.8. Note that the *N. brevirostris RH2B* gene is placed in-between the percomorph *RH2A* and *RH2B* clades (also see Fig. 5). *RH1* = rhodopsin 1 (rod opsin), *RH2* = rhodopsin 2, *SWS2* = short-wavelength-sensitive 2, *LWS* = long-wavelength-sensitive, *va* = vertebrate ancient opsin (outgroup), scalebar = substitution per site. A detailed phylogeny and GenBank accession numbers are shown in Fig. S4.

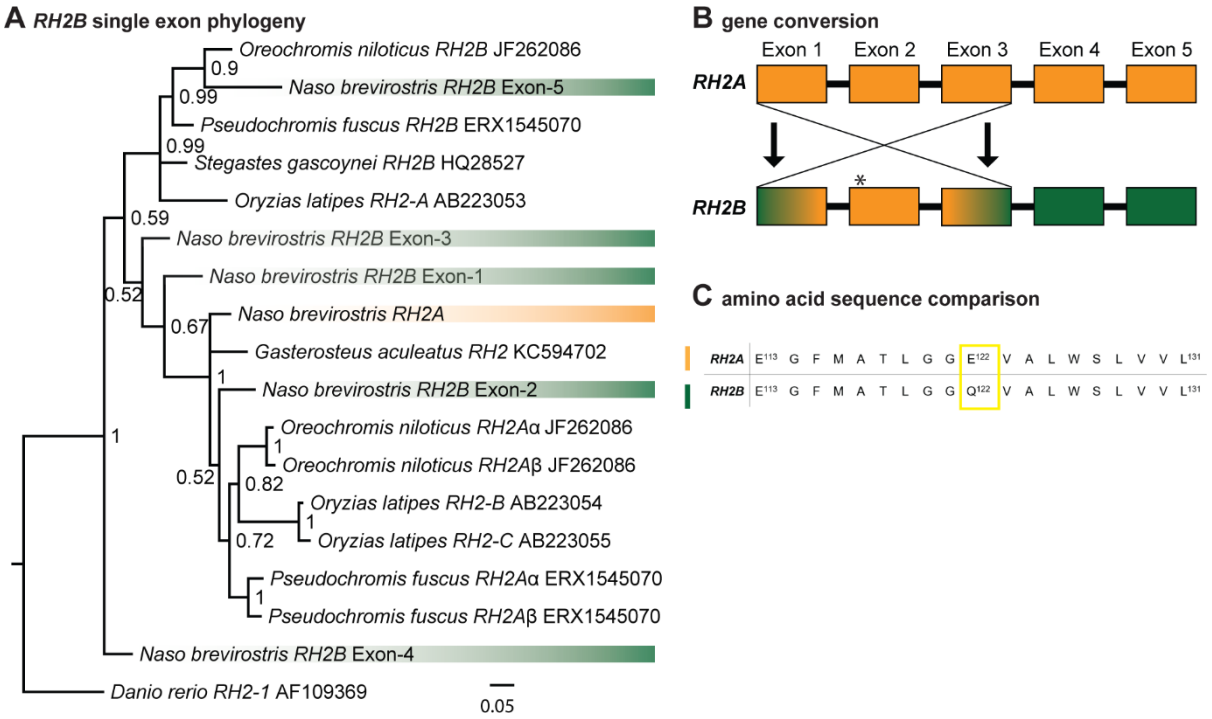

Fig. 5 Single-exon green opsin (*RH2*) phylogeny. (A) Using the single exons (green) of the *N. brevirostris RH2B* gene revealed that exons 3-5 cluster within or close to the percomorph *RH2B* clade, whereas exons 1 and 2 cluster close to or within the *RH2A* clade (*N. brevirostris RH2A* in yellow). Note that *Oryzias latipes* genes have a different nomenclature in comparison to the other fish opsin genes. Nodes denote Bayesian posterior probabilities. (B) Illustration of the relationship between the two *RH2* paralogs of *N. brevirostris* based on the single-exon *RH2B* phylogeny. The suggested gene conversion from *RH2A* into Exons 1-3 of *RH2B* makes it near impossible to resolve its phylogenetic position if considering the whole coding region of the gene (also see Fig. 4, Fig. S4). The asterisk marks the approximate position of the amino acid residue 122 in RH2B. C) RH2A and RH2B amino acid sequence alignments for residues 113-131 (according to bovine rhodopsin). Note that site 122 in RH2B, despite lying with the gene conversion region, shows the RH2B specific, shorter shifted 122Q (Chinen et al. 2005).

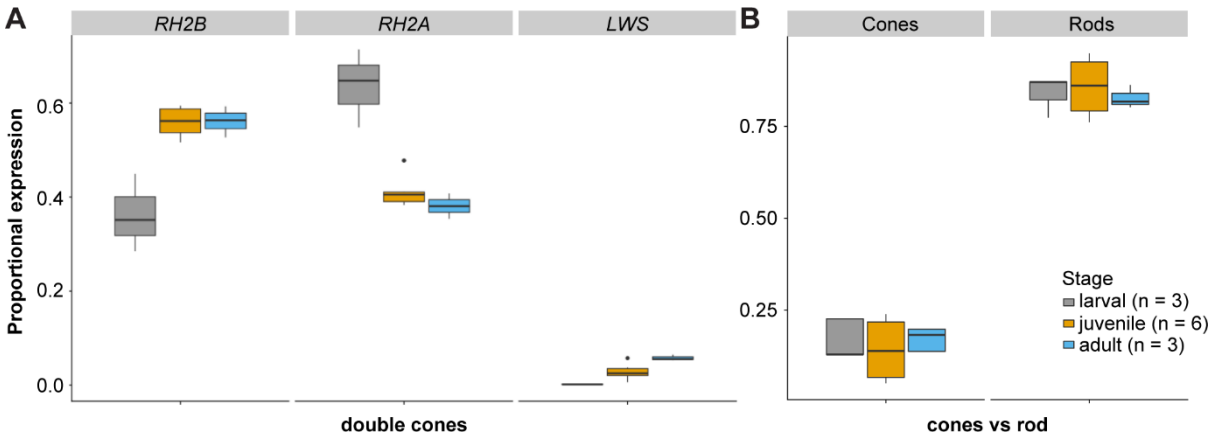

Fig. 6 Proportional expression of *N. brevirostris* opsin genes. (A) Independent of ontogenetic stage, *N. brevirostris* expressed the *SWS2B* single cone (100% of single cone expression; see Table S2 for details) and three double cone opsin genes: *RH2B*, *RH2A*, and *LWS*. The proportional expression of double cone opsins revealed a change in expression of the two *RH2* genes between the larval and the juvenile stage as well as a steady increase in the expression of *LWS* with development. (B) The proportional expression of cone (*SWS2B*, *RH2B*, *RH2A*, *LWS*) versus rod opsin (*RH1*) remained similar throughout ontogeny. The box indicates Q2 and Q3, with the line indicating the median and the whiskers indicating Q1 and Q4 of the data.

Supplementary Material

Table S1 Summary of the stereology parameters used for the analysis of ganglion cell and photoreceptor cell distributions along with Schaeffer's coefficient of error (CE).

Ganglion cells							
Stage	Individual	SL, cm	Lens ∅, mm	Counting Frame size, µm	Grid size, µm	Site No.	Schaeffer's CE
Adult	ID1	30.6	6.6	90 x 90	1350 x 1350	219	0.042
	ID2	30.8	6.9	90 x 90	1350 x 1350	238	0.041
Juvenile	ID1	13.8	4.7	80 x 80	1000 x 1000	225	0.042
	ID2	15.2	4.9	80 x 80	1000 x 1000	209	0.041
	ID3	15.7	4.5	80 x 80	1000 x 1000	185	0.042
Larval	ID1	3.18	1.4	50 x 50	250 x 250	205	0.034
Photoreceptors							
Stage	Individual	SL, cm	Lens ∅, mm	Counting Frame size, µm	Grid size, µm	Site N	Schaeffer's CE
Adult	ID3	29.7	6.8	90 x 90	1450 x 1450	207	0.047
	ID4	27.7	6.4	90 x 90	1450 x 1450	185	0.050
Juvenile	ID3	13.8	4.5	80 x 80	950 x 950	195	0.045
	ID4	18.5	5.6	80 x 80	950 x 950	210	0.054
Larval	ID2	3.08	1.6	45 x 45	340 x 340	216	0.051
	ID3	3.30	1.5	45 x 45	340 x 340	208	0.053

SL = standard length; ∅ = diameter.

Table S2: Summary of transcriptomes of *N. brevirostris*, opsin mapping (incl. base pair coverage), and proportional opsin gene expression.

RH1 = rod opsin, *SWS2* = short-wavelength sensitive 2, *RH2* = rhodopsin like 2, *LWS* = long-wavelength sensitive

		RNA sequencing			Mapping					Proportional opsin expression % (normalized to coding sequence length)					
		Transcriptome			Rod	Single cones (SC)	Double cones (DC)			Rod vs Cone		SC	DC		
Stage	ID	Standard length (cm)	# raw reads	# filtered reads	*RH1* # reads	*SWS2B* # reads	*RH2B* # reads	*RH2A* # reads	*LWS* # reads	R	C	*SWS2B*	*RH2B*	*RH2A*	*LWS*
Larval	L19	3.18	25,789,980	22,792,356	1,178,462	35,634	39,634	98,812	188	87.1	12.9	100	28.5	71.4	0.1
	L20	3.07	24,433,162	21,718,144	1,125,563	35,125	46,386	84,954	158	87.1	12.9	100	35.2	64.7	0.1
	L26	3.07	25,820,192	22,996,270	1,066,043	47,843	118,750	143,946	602	77.4	22.6	100	45	54.8	0.2
	Mean		**25,347,778**	**22,502,257**	**1,123,356**	**39,534**	**68,257**	**109,237**	**316**	**83.9**	**16.1**	**100**	**36.2**	**63.6**	**0.2**
	Se		**457,391**	**396,451**	**32,471**	**4,157**	**25,321**	**17,809**	**143**	**3.23**		**-**	**4.8**	**4.8**	**0.0**
Juvenile	FD8	6.5	14,854,726	13,176,755	679,634	39,829	88,651	57,481	3,005	78.2	21.8	100	59.3	38.7	2
	SRG1	15.5	9,043,423	7,458,565	365,928	17,873	34,235	25,225	2,333	82.1	17.9	100	55.3	41	3.7
	SRG21	19.5	9,895,137	6,536,514	631,856	6,452	15,656	10,926	786	94.9	5.1	100	57.1	40.1	2.8
	SRG22	15.2	12,990,170	11,708,074	612,536	11,203	17,282	13,292	1,887	93.3	6.7	100	53.1	41.1	5.8
	SRG28	14.2	2,914,410	2,560,493	133,236	8,445	19,856	12,731	748	76.1	23.9	100	59.5	38.3	2.2
	SRG31_2	15.3	20,785,172	18,299,205	896,430	18,684	41,142	37,840	466	90.1	9.9	100	51.7	47.7	0.6
	Mean		**11,747,173**	**9,956,601**	**553,270**	**17,081**	**36,137**	**26,249**	**1,537.5**	**85.8**	**14.2**	**100**	**56.0**	**41.2**	**2.8**
	Se		**2,460,660**	**2,277,979**	**108,772**	**4,976**	**11,294**	**7,519.4**	**418.1**	**3.3**		**-**	**1.3**	**1.4**	**0.7**
Adult	SRG2_VT	33.0	21,687,092	17,535,898	1,555,234	75,996	173,683	116,779	17,268	80.2	19.8	100	56.3	38.1	5.6
	SRG4_VT	30.8	13,659,085	12,284,294	1,454,916	72,354	94,914	56,266	8,520	86.2	13.8	100	59.3	35.4	5.3
	SRG7_VT	30.6	22,826,459	18,406,216	1,817,211	76,589	173,392	133,336	21,603	81.8	18.2	100	52.7	40.8	6.5
	Mean		**19,390,879**	**16,075,469**	**1,609,120**	**74,980**	**147,330**	**102,127**	**15,797.0**	**82.7**	**17.3**	**100**	**56.1**	**38.1**	**5.8**
	Se		**2,884,709**	**1,912,165**	**108,000**	**1,324**	**26,208**	**23,423.3**	**3,847.7**	**1.8**		**-**	**1.9**	**1.6**	**0.4**

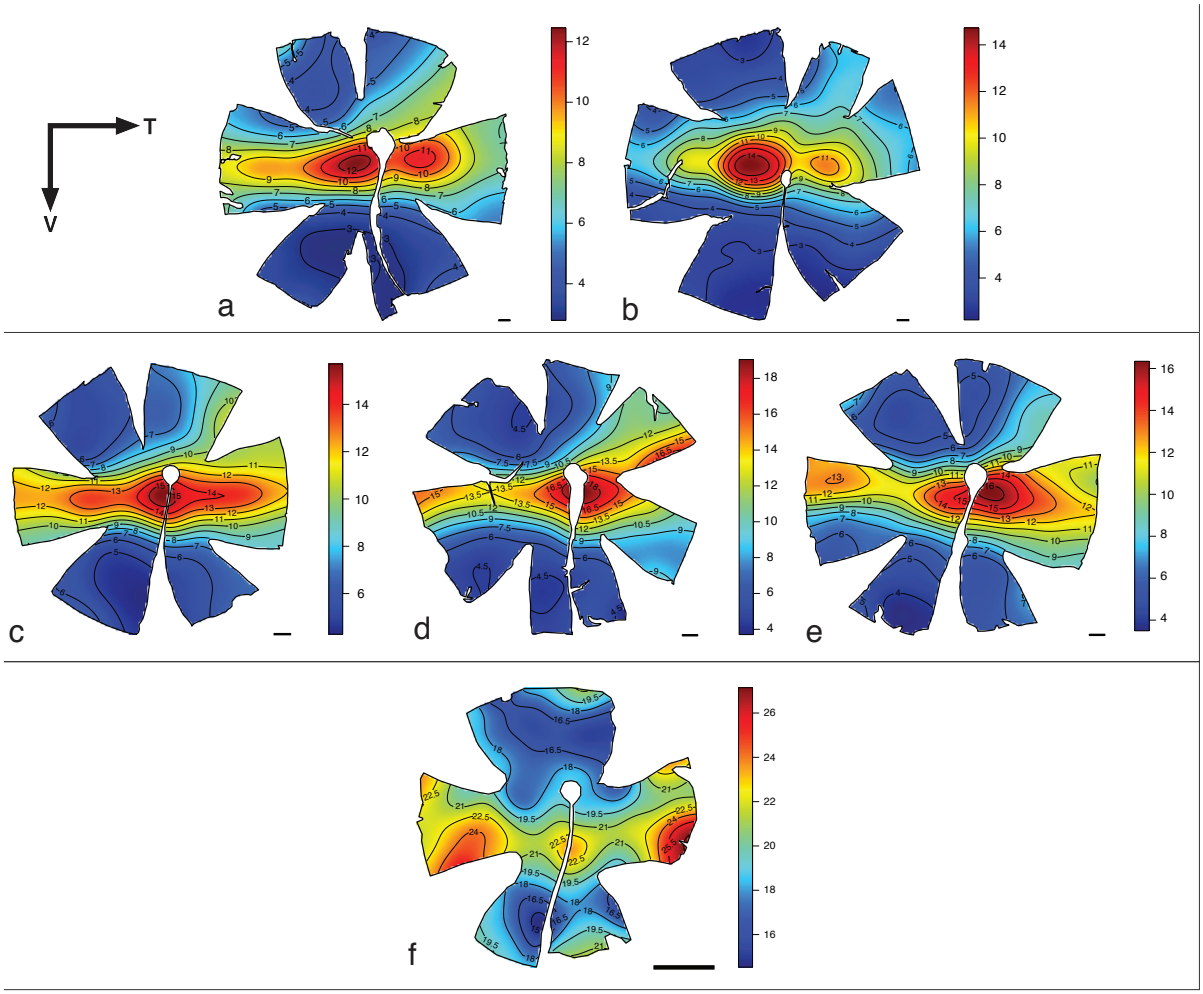

Fig. S1: Topographic distribution of retinal ganglion cells for adult (a, b), juvenile (c, d, e), and larval (f) stages. Black lines represent isodensity contours, and values are expressed in densities x 10^3 cells/mm^2. V = Ventral, T = temporal. Scale bar = 1 mm.

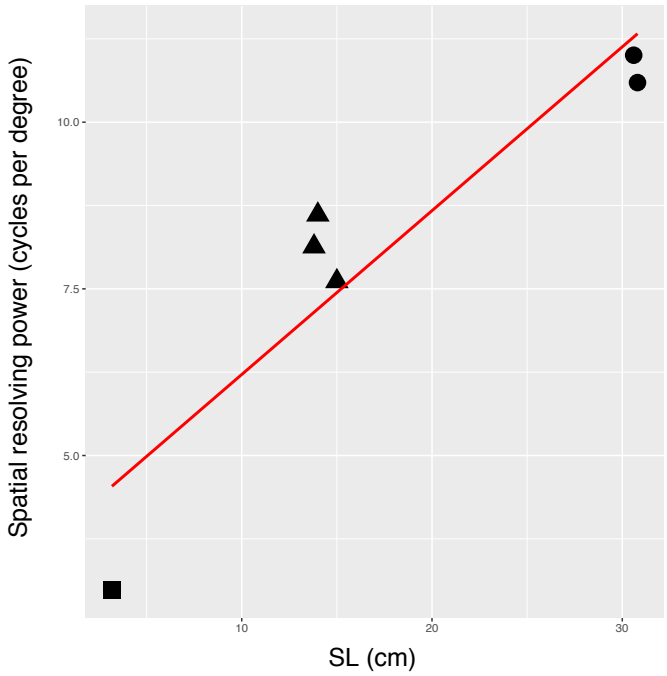

Fig. S2 Relationship between visual acuity **(**spatial resolving power) and body size (standard length, SL) for different life stages of *Naso brevirostris*. Squares = larval stage; triangles = juvenile stage; circles = adult stage.

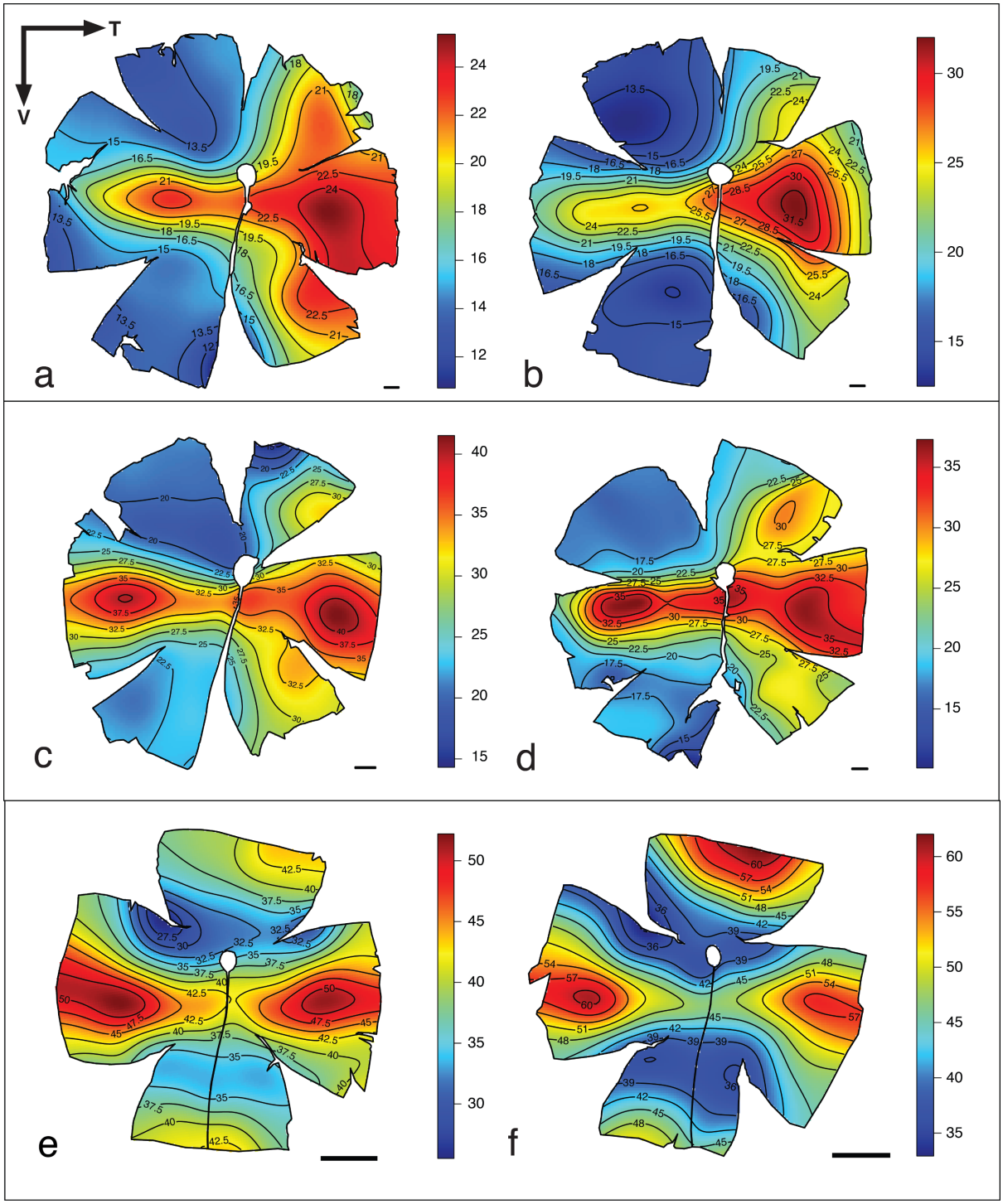

Fig. S3: Topographic distribution of total cone photoreceptors for adult (a, b), juvenile (c, d), and larval (e, f) stages. The topographic maps for single and double cones for all individuals are provided on Dryad. Black lines represent isodensity contours, and values are expressed in densities x 10^3 cells/mm^2. V = Ventral, T = temporal. Scale bar = 1 mm.

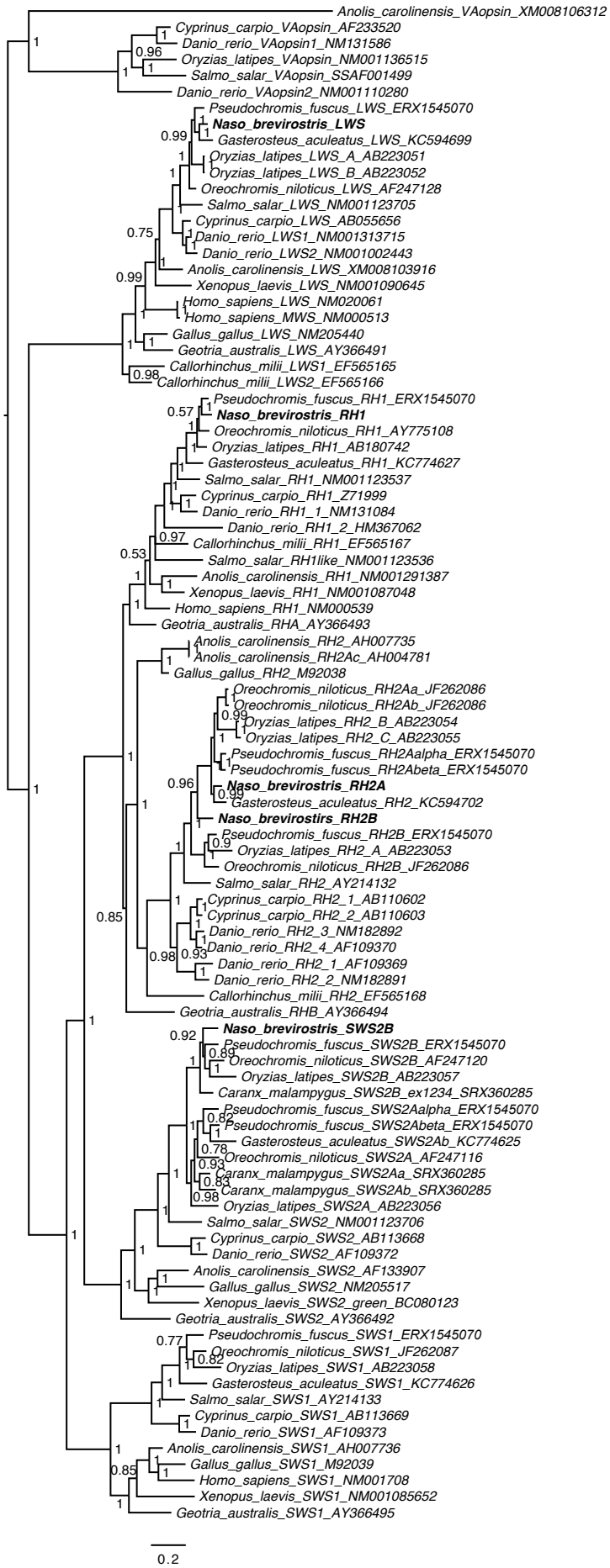

Fig. S4: Vertebrate opsin phylogeny. The different *Naso brevirostris* opsins (extracted from the transcriptomes) are shown in bold. Bayesian support values as indicated. *RH1* = rhodopsin 1 (rod opsin), *RH2* = rhodopsin 2, *SWS2* = short-wavelength-sensitive 2, *SWS1* = short-wavelength-sensitive 1, *LWS* = long-wavelength-sensitive, *va* = vertebrate ancient opsin (outgroup), scalebar = substitution per site.

Supplementary Material

Table S1 Summary of the stereology parameters used for the analysis of ganglion cell and photoreceptor cell distributions along with Schaeffer's coefficient of error (CE).

Ganglion cells							
Stage	Individual	SL, cm	Lens ∅, mm	Counting Frame size, µm	Grid size, µm	Site No.	Schaeffer's CE
Adult	ID1	30.6	6.6	90 x 90	1350 x 1350	219	0.042
	ID2	30.8	6.9	90 x 90	1350 x 1350	238	0.041
Juvenile	ID1	13.8	4.7	80 x 80	1000 x 1000	225	0.042
	ID2	15.2	4.9	80 x 80	1000 x 1000	209	0.041
	ID3	15.7	4.5	80 x 80	1000 x 1000	185	0.042
Larval	ID1	3.18	1.4	50 x 50	250 x 250	205	0.034
Photoreceptors							
Stage	Individual	SL, cm	Lens ∅, mm	Counting Frame size, µm	Grid size, µm	Site N	Schaeffer's CE
Adult	ID3	29.7	6.8	90 x 90	1450 x 1450	207	0.047
	ID4	27.7	6.4	90 x 90	1450 x 1450	185	0.050
Juvenile	ID3	13.8	4.5	80 x 80	950 x 950	195	0.045
	ID4	18.5	5.6	80 x 80	950 x 950	210	0.054
Larval	ID2	3.08	1.6	45 x 45	340 x 340	216	0.051
	ID3	3.30	1.5	45 x 45	340 x 340	208	0.053

SL = standard length; ∅ = diameter.

Table S2: Summary of transcriptomes of *N. brevirostris*, opsin mapping (incl. base pair coverage), and proportional opsin gene expression.

RH1 = rod opsin, *SWS2* = short-wavelength sensitive 2, *RH2* = rhodopsin like 2, *LWS* = long-wavelength sensitive

		RNA sequencing			Mapping					Proportional opsin expression % (normalized to coding sequence length)					
		Transcriptome			Rod	Single cones (SC)	Double cones (DC)			Rod vs Cone		SC	DC		
Stage	ID	Standard length (cm)	# raw reads	# filtered reads	*RH1* # reads	*SWS2B* # reads	*RH2B* # reads	*RH2A* # reads	*LWS* # reads	R	C	*SWS2B*	*RH2B*	*RH2A*	*LWS*
Larval	L19	3.18	25,789,980	22,792,356	1,178,462	35,634	39,634	98,812	188	87.1	12.9	100	28.5	71.4	0.1
	L20	3.07	24,433,162	21,718,144	1,125,563	35,125	46,386	84,954	158	87.1	12.9	100	35.2	64.7	0.1
	L26	3.07	25,820,192	22,996,270	1,066,043	47,843	118,750	143,946	602	77.4	22.6	100	45	54.8	0.2
	Mean		**25,347,778**	**22,502,257**	**1,123,356**	**39,534**	**68,257**	**109,237**	**316**	**83.9**	**16.1**	**100**	**36.2**	**63.6**	**0.2**
	Se		**457,391**	**396,451**	**32,471**	**4,157**	**25,321**	**17,809**	**143**	**3.23**		**-**	**4.8**	**4.8**	**0.0**
Juvenile	FD8	6.5	14,854,726	13,176,755	679,634	39,829	88,651	57,481	3,005	78.2	21.8	100	59.3	38.7	2
	SRG1	15.5	9,043,423	7,458,565	365,928	17,873	34,235	25,225	2,333	82.1	17.9	100	55.3	41	3.7
	SRG21	19.5	9,895,137	6,536,514	631,856	6,452	15,656	10,926	786	94.9	5.1	100	57.1	40.1	2.8
	SRG22	15.2	12,990,170	11,708,074	612,536	11,203	17,282	13,292	1,887	93.3	6.7	100	53.1	41.1	5.8
	SRG28	14.2	2,914,410	2,560,493	133,236	8,445	19,856	12,731	748	76.1	23.9	100	59.5	38.3	2.2
	SRG31_2	15.3	20,785,172	18,299,205	896,430	18,684	41,142	37,840	466	90.1	9.9	100	51.7	47.7	0.6
	Mean		**11,747,173**	**9,956,601**	**553,270**	**17,081**	**36,137**	**26,249**	**1,537.5**	**85.8**	**14.2**	**100**	**56.0**	**41.2**	**2.8**
	Se		**2,460,660**	**2,277,979**	**108,772**	**4,976**	**11,294**	**7,519.4**	**418.1**	**3.3**		**-**	**1.3**	**1.4**	**0.7**
Adult	SRG2_VT	33.0	21,687,092	17,535,898	1,555,234	75,996	173,683	116,779	17,268	80.2	19.8	100	56.3	38.1	5.6
	SRG4_VT	30.8	13,659,085	12,284,294	1,454,916	72,354	94,914	56,266	8,520	86.2	13.8	100	59.3	35.4	5.3
	SRG7_VT	30.6	22,826,459	18,406,216	1,817,211	76,589	173,392	133,336	21,603	81.8	18.2	100	52.7	40.8	6.5
	Mean		**19,390,879**	**16,075,469**	**1,609,120**	**74,980**	**147,330**	**102,127**	**15,797.0**	**82.7**	**17.3**	**100**	**56.1**	**38.1**	**5.8**
	Se		**2,884,709**	**1,912,165**	**108,000**	**1,324**	**26,208**	**23,423.3**	**3,847.7**	**1.8**		**-**	**1.9**	**1.6**	**0.4**

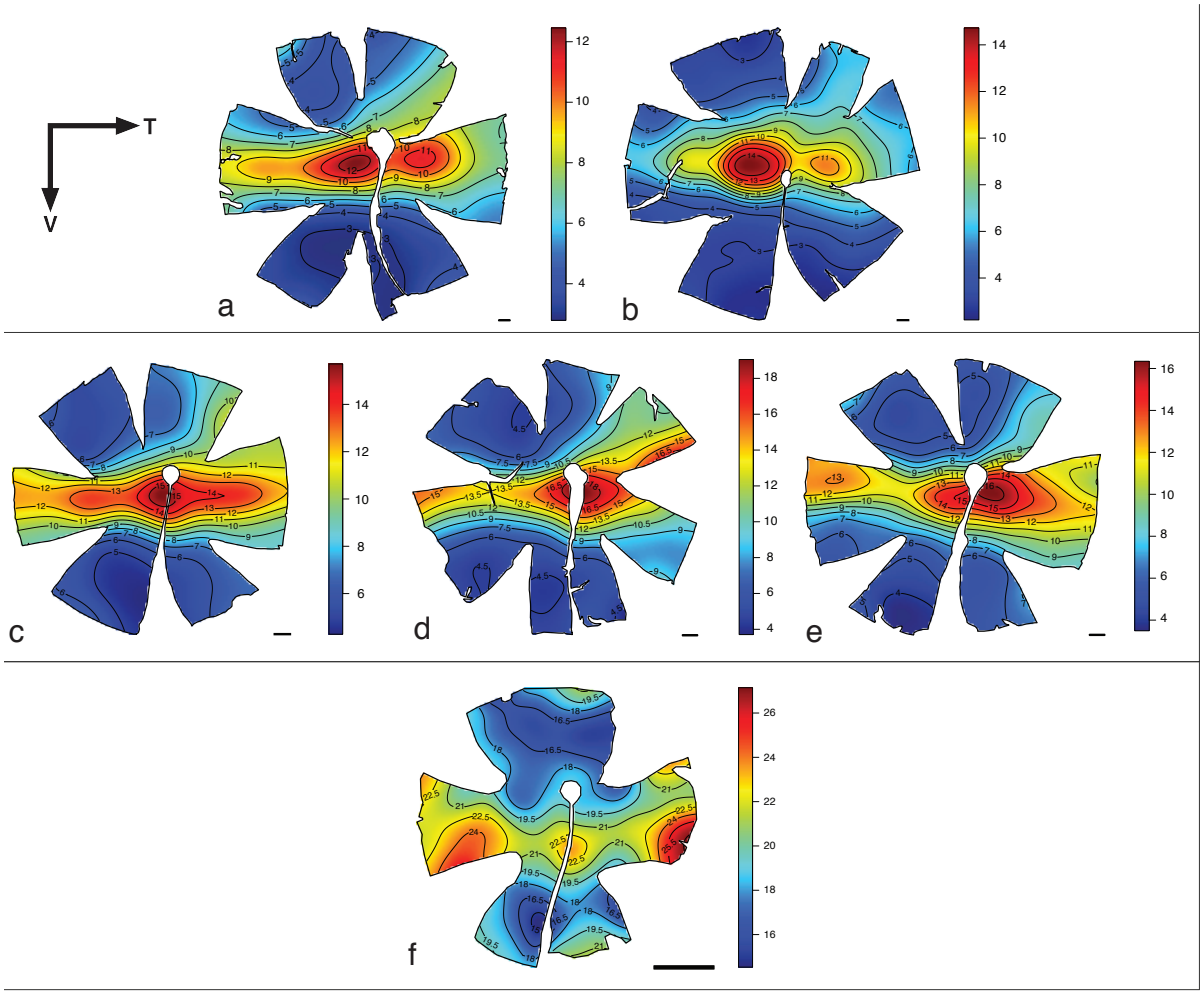

Fig. S1: Topographic distribution of retinal ganglion cells for adult (a, b), juvenile (c, d, e), and larval (f) stages. Black lines represent isodensity contours, and values are expressed in densities x 10^3 cells/mm^2. V = Ventral, T = temporal. Scale bar = 1 mm.

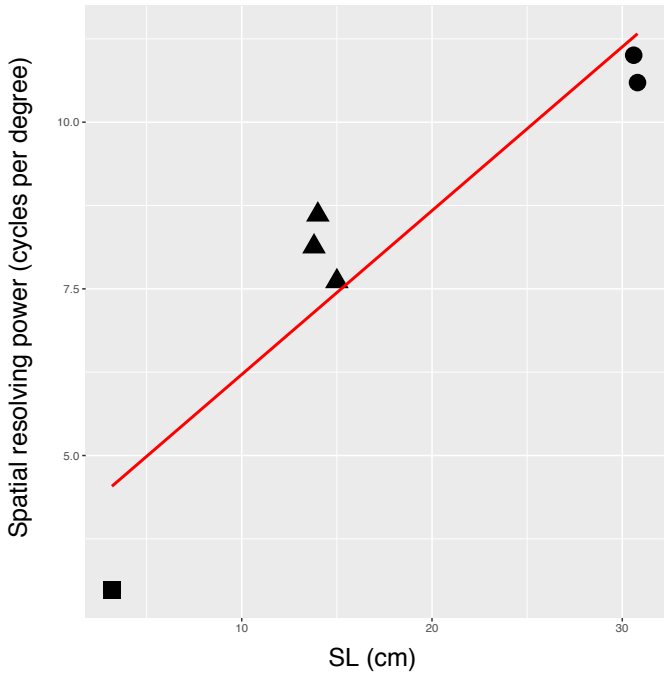

Fig. S2 Relationship between visual acuity **(**spatial resolving power) and body size (standard length, SL) for different life stages of *Naso brevirostris*. Squares = larval stage; triangles = juvenile stage; circles = adult stage.

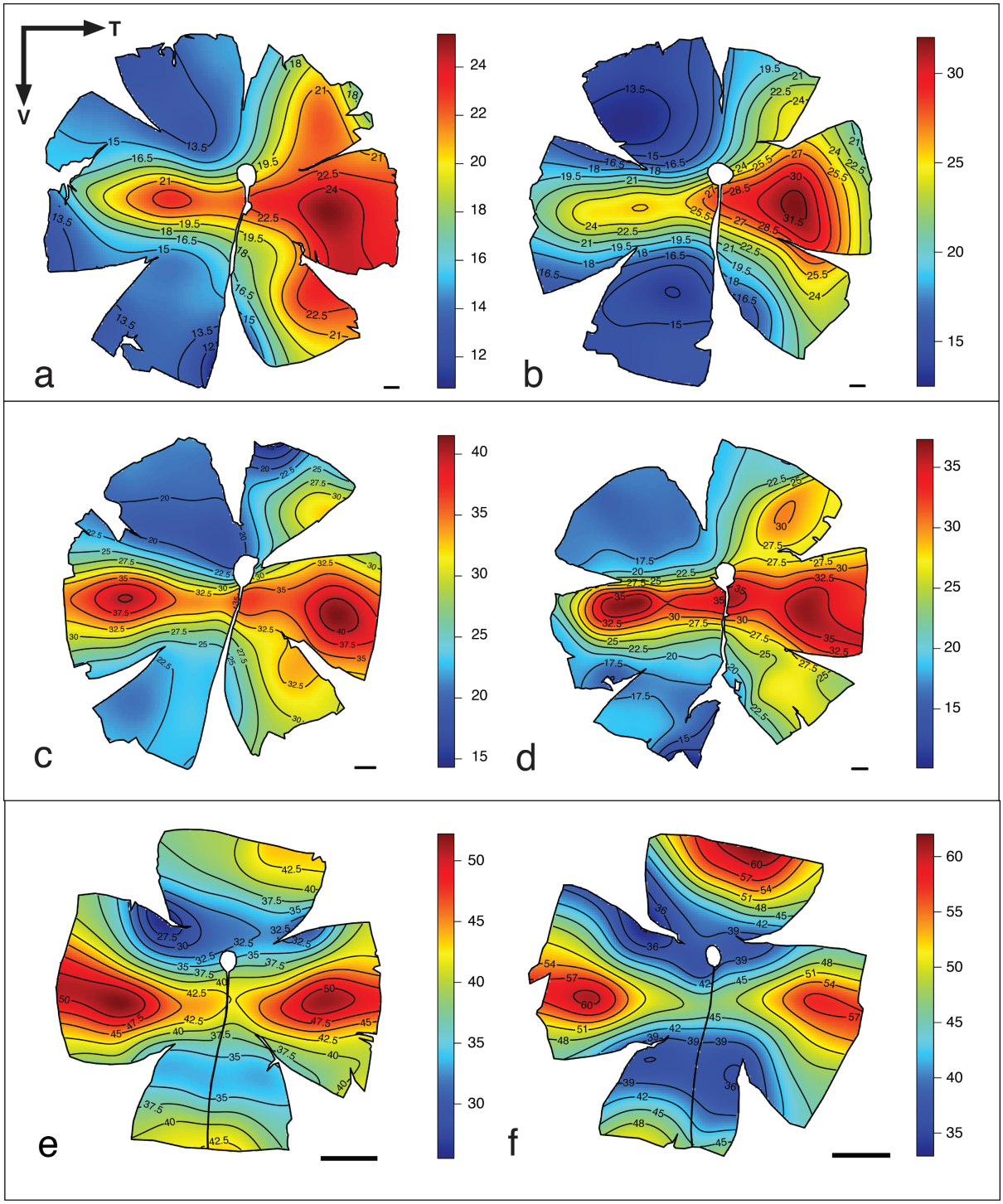

Fig. S3: Topographic distribution of total cone photoreceptors for adult (a, b), juvenile (c, d), and larval (e, f) stages. The topographic maps for single and double cones for all individuals are provided on Dryad. Black lines represent isodensity contours, and values are expressed in densities x 10^3 cells/mm^2. V = Ventral, T = temporal. Scale bar = 1 mm.

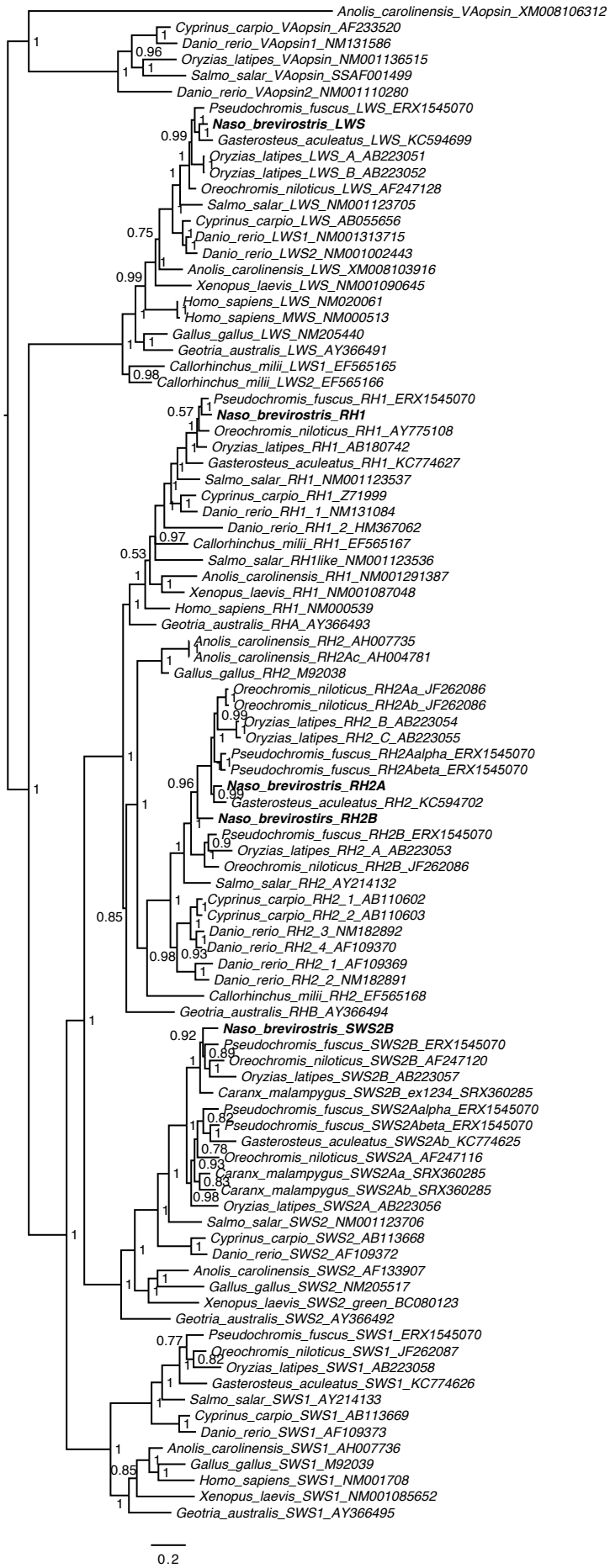

Fig. S4: Vertebrate opsin phylogeny. The different *Naso brevirostris* opsins (extracted from the transcriptomes) are shown in bold. Bayesian support values as indicated. *RH1* = rhodopsin 1 (rod opsin), *RH2* = rhodopsin 2, *SWS2* = short-wavelength-sensitive 2, *SWS1* = short-wavelength-sensitive 1, *LWS* = long-wavelength-sensitive, *va* = vertebrate ancient opsin (outgroup), scalebar = substitution per site.